



TAMPEREEN TEKNILLINEN YLIOPISTO  
TAMPERE UNIVERSITY OF TECHNOLOGY

**MARCELO FABIÁN TRUJILLO FIERRO  
TESTBED DESIGN AND IMPLEMENTATION  
FOR WIRELESS POWER TRANSFER  
USING SOFTWARE-DEFINED RADIOS**

Master of Science thesis

Examiners: Dr. Taneli Riihonen  
and Dr. Markus Allén  
Examiners and topic approved by the  
Faculty Council of the Faculty of  
Computing and Electrical  
Engineering  
on 8th August 2018

## ABSTRACT

**MARCELO FABIÁN TRUJILLO FIERRO:** Testbed Design And Implementation For Wireless Power Transfer Using Software-Defined Radios

Tampere University of Technology

Master of Science thesis, 82 pages

November 21st 2018

Master's Degree Programme in Electrical Engineering

Major: Wireless Communications

Examiners: Dr. Taneli Riihonen and Dr. Markus Allén

Keywords: RF, WPT, testbed, SDR, RF-to-DC, SWIPT, WIPT

The area of wireless power transfer (WPT) dates back more than a century. This capability to transfer power without wires gives also motive for harvesting resources that have not yet been considered, such as the RF signals that cellular networks employ to send information. Only a while ago the research in the WPT field was focused on improving the elements in the power transmission chains separately. However, in recent years, such closed-loop schemes have emerged that have the potential to improve the efficiency of the entire system by adapting key elements in the chain together, such as the transmitted waveform and the rectenna performance. The scope of the thesis aims to contribute to the ultimate objective of merging information and power transfer in a simultaneous wireless information and power transfer/transmission (SWIPT) network.

The main objective of this thesis is to design and implement a testbed for research on WPT and SWIPT. A closed-loop system is implemented for future scientific experiments for broadcasting a given radio signal and at the same time measuring the total power that an energy receiver will harvest from the transmission. The main element of the testbed is a computer from which master program controlling the transmission, the synchronization, and reading of the harvested voltage. The master program is written in C++ language and is designed to transmit with a USRP and receive voltage readings from the harvesting energy receivers that consist of RF-to-DC converter, ADC and Arduino microcontroller. Results show that the implemented testbed works as planned, and the master program can perform adaptive algorithms. Furthermore, the testbed can be used for experiments for any given waveform meant for communications, WPT, and SWIPT.

## PREFACE

This thesis works as a guide and a manual for the testbed that was carried out during summer-autumn of 2018 in the Tampere University of Technology (TUT) facilities, specifically in the laboratories of the Department of Electronics and Communication Engineering.

A special acknowledgment to my supervisor, Taneli Riihonen, for having given me the opportunity to work on this project, and for having entrusted me with such a complex and interesting task of developing a research testbed. The tremendous support and guidance that Taneli gave me during the thesis motivated me to give all my effort and dedication to the project. I would also like to thank Markus Allén and his immense contribution to this thesis. If he was not helping in the hardware implementation, he was always willing to talk and give new ideas.

My total gratitude to the people in TUT who helped me with the implementation or the writing process, like Adrian Benfield, whose tremendous support for the writing process taught me to accept self-criticism and helped me improve my thesis. The TELOK electronic club, I was lucky they found me and wanted to help me. Also, the NISEC group, whose door was always open for my doubts about Linux; César Pereida García, Sohaib ul Hassan, Alejandro Cabrera Alaya, and a special mention for Nicola Tuveri and his endless patience. My office mates, and people in the department; Mohammad Hosseinovad, Pablo Pascual, Nachiket Ayir, Jarkko Laaja, and Ronal Bejarano Rodriguez who helped in the thesis writing and also to maintain the optimism.

I would also like to thank my loving and supporting parents. Although the long distance in between us, they are always with me. In addition, to my brother who has always answered when I ask for guidance. Last but not least, I dedicate this thesis to my wife and son, whose support has been beyond the limits. They are the main reason for most of my decisions in life. I take the opportunity to give the credits of the photos to my wife Henrietta.

Tampere, 21.11.2018

**Marcelo Fabián Trujillo Fierro**

*"Artifex vitae, artifex sui"*

# CONTENTS

1. Introduction . . . . .	1
1.1 Background And Motivation . . . . .	1
1.2 Objectives And Scope . . . . .	2
1.3 Thesis Structure . . . . .	3
2. Wireless Power Transfer . . . . .	5
2.1 Radio Wave Power Transmission . . . . .	5
2.1.1 Microwave Power Transmission System . . . . .	9
2.1.2 Microwave Power Transfer Applications . . . . .	11
2.2 RF Wireless Power Transfer Systems . . . . .	15
2.2.1 Requirements And Challenges For A Power Network . . . . .	16
2.2.2 Design For Far-Field RF WPT System . . . . .	17
2.2.3 WPT Signal And System Design . . . . .	20
2.2.4 Wireless Power And Wireless Information Integration . . . . .	23
2.3 WPT Prototypes In The Literature . . . . .	24
3. Digital Communications . . . . .	28
3.1 I/Q Modulation And Constellation Representation . . . . .	29
3.2 Multicarrier modulation And OFDM . . . . .	31
3.3 Power Amplification And Nonlinearity . . . . .	34
4. Testbed Structure . . . . .	37
4.1 Transmitter Side . . . . .	37
4.1.1 Software Defined Radio (SDR), USRP . . . . .	38
4.1.2 Power Meter . . . . .	39
4.2 Receiver Side . . . . .	41
4.2.1 RF-to-DC Converter, Power harvester <sup>®</sup> . . . . .	41
4.2.2 Analog-to-Digital converter, ADS1115 . . . . .	43
4.2.3 Microcontroller, Arduino Nano . . . . .	44
4.3 Final Transmitter Structure . . . . .	46

4.4	Final Receiver Structure . . . . .	46
4.5	Final Testbed Implementation . . . . .	48
4.6	TestBed Software . . . . .	49
4.6.1	Main Program . . . . .	49
4.6.2	Subprogram In Microcontroller . . . . .	54
5.	Testbed Functionality . . . . .	57
5.1	Setting Parameters . . . . .	57
5.2	File Transmission Mode . . . . .	58
5.3	Vector Transmission Mode . . . . .	59
5.4	Program Execution . . . . .	60
5.5	Obtained Data . . . . .	62
6.	Operational Assessments . . . . .	65
6.1	File Transmission Assessments . . . . .	66
6.2	Vector Transmission Assessments . . . . .	68
6.3	Receiver Side Assessments . . . . .	70
7.	Conclusions . . . . .	72

## LIST OF FIGURES

1.1	General project diagram . . . . .	3
2.1	First advances in radio wave power transmission . . . . .	6
2.2	Early beginnings in the power transfer using radio waves . . . . .	7
2.3	Block diagram, microwave power transmission system based. . . . .	10
2.4	RFID tags diagram . . . . .	11
2.5	Proposal for charging EV via an MPT system. . . . .	12
2.6	Stationary High Altitude Relay Platform (SHARP) . . . . .	13
2.7	Solar power satellites configuration . . . . .	14
2.8	Block diagram for a general far-field WPT transmission . . . . .	16
2.9	Architecture for an improved far-field WPT transmission . . . . .	20
2.10	Networks diagram for RF WPT . . . . .	22
3.1	Basic digital chain diagram . . . . .	28
3.2	I/Q modulation block diagram . . . . .	30
3.3	Complex Constellation . . . . .	30
3.4	Subchannels within a bandwidth . . . . .	31
3.5	OFDM signal, sinc-shaped pulses . . . . .	32
3.6	General block diagram for a OFDM system . . . . .	33
3.7	PA models, relation between input/output . . . . .	35
3.8	Nonlinear system example . . . . .	36
4.1	NI USRP-2900 transmitter block diagram . . . . .	39

4.2	Devices for supplied power measurements . . . . .	40
4.3	P2110 and P1110 EVBs . . . . .	41
4.4	P2110 and P1110 EVBs . . . . .	42
4.5	ADS1115 hardware . . . . .	43
4.6	Arduinbo hardware . . . . .	45
4.7	Final testbed transmitter structure . . . . .	46
4.8	Wire schematics for the receiver hardware design. . . . .	47
4.9	Receiver structure implementation. . . . .	48
4.10	Final testbed setup . . . . .	48
4.11	C++ main program diagram . . . . .	51
4.12	Measurements to calculate delay in the receiver side . . . . .	53
4.13	Arduino main program structure diagram . . . . .	56
5.1	File to configure testbed parameters . . . . .	57
5.2	Program execution diagram . . . . .	60
5.3	Terminal setting of USRP parameters . . . . .	61
5.4	Folder with the testbed main program and folders . . . . .	62
5.5	Terminal output after transmission is over . . . . .	62
5.6	Summary text created after transmission . . . . .	63
6.1	Wired operational assessments of the testbed . . . . .	65
6.2	1 MHz complex tone . . . . .	66
6.3	File transmission operational assessments . . . . .	67
6.4	Vector transmission operational assessments . . . . .	69
6.5	Operational assessments for the receiver side . . . . .	71

## LIST OF TABLES

2.1	Main WPT milestone in recent history [1]. . . . .	8
2.2	Summary and comparison between WPT technologies [1]. . . . .	9
2.3	Comparison for different diodes used in a rectenna. . . . .	11
2.4	Summary of implemented prototypes in RF WPT research . . . . .	25
4.1	USRP 2900, Transmitter characteristics. . . . .	38
4.2	USB power meter ZY1273 specifications. . . . .	40
4.3	Switch selection for RSSI mode at the EVBs. . . . .	42
4.4	Identifier for every EVB used in the testbed. . . . .	43
4.5	ADS1115 maximum values. . . . .	44
4.6	ADS1115 PGA scale. . . . .	44
4.7	Arduino Nano specifications. . . . .	45
4.8	Notebook computer specifications used in testbed. . . . .	49
4.9	Installation of the UHD dependencies and repository. . . . .	50
4.10	Example of the Arduino serialprint. . . . .	55
6.1	The output power at the USRP vs the gain selected in the parameters	68
6.2	Results obtained for operational assessments at the receiver side. . . .	70

## LIST OF ABBREVIATIONS AND SYMBOLS

5G	5 <sup>th</sup> generation wireless systems
ADC	Analog-to-Digital Converter
DC	Direct Current
DFT	Discrete Fourier Transform
EVB	Evaluation Board
FFT	Fast Fourier Transform
FPGA	Field-Programmable Gate Array
IDFT	Inverse Discrete Fourier Transform
IFFT	Inverse-Fast Fourier Transform
IoT	Internet of things
MATLAB	Matrix laboratory, programming environment by Mathworks <sup>®</sup>
MPT	Microwave Power Transfer
OFDM	Orthogonal Frequency-Division Multiplexing
PAPR	Peak-to-Average Power Ratio
RF	Radio-frequency
RFID	Radio-Frequency Identification
SDR	Software-defined Radio
SWIPT	Simultaneous Wireless Information and Power Transfer/Transmission
UHD	USRP Hardware Device
USB	Universal Serial Bus
USRP	Universal Software Radio Peripheral
WIPT	Wireless Information and Power Transfer/Transmission
WPT	Wireless power transfer
$\pi$	constant pi, ratio of the circumference of a circle by its diameter
$dB$	decibel
$j$	imaginary unit
$f$	frequency
$f_c$	carrier frequency
$t$	time
$w_c$	angular carrier frequency
$w$	angular frequency
$x_{sat}$	saturation threshold
$X(k)$	signal in frequency domain
$x(t)$	signal in time domain

# 1. INTRODUCTION

This Chapter presents the introduction to the thesis, which consists of three main sections: background and motivation in Section 1.1, the objectives and scope in Section 1.2, and finally the structure of the thesis in Section 1.3.

## 1.1 Background And Motivation

The first attempts at energy transfer using a wireless approach started more than one hundred years, with the Wardencliffe Tower (in 1904) being one of the most famous of these projects. As [2] points out, the extraordinary mind of Nikola Tesla knew that wireless power transfer was viable and could be a tremendous boon for mankind. Since those early experiments at the beginning of the 19th century, many years have passed and recent developments in the wireless power transfer field (WPT) have now made this technology part of everyday life, used in applications such as the Radio-Frequency Identification (RFID) tags used in many commercial systems [3].

There are different methods for transmitting power without cables [4]. The ordinary consumer is already familiar with applications such as charger docks for smartphones, which couple magnetic fields over short distances in order to achieve the wireless transmission of energy. On the other hand, energy can be transmitted over longer distances by sending electromagnetic signals from a transmitter to a receiver. Such microwave power transmission (MPT) has been used for charging unmanned airborne vehicles (UAV), and there are plans to send energy to Earth from orbiting satellites that collect solar radiation (solar power satellites). On a less ambitious scale, RFID tags also work with the MPT technique [5].

As a result of the successful adoption of MPT by the market, research is now starting to focus on more significant scaled applications, and the idea of integrating it with wireless information transfer has stimulated an exciting and promising area of research [6]. So far, it is the attenuation in wireless propagation which has confined this technology mainly to short distance transmission ranges. However, thanks to the advent of a 5<sup>th</sup> generation of cellular networks (5G), i.e. small cell networks and

enhanced MIMO (Multiple-Input Multiple-Output) systems [2], WIPT (Wireless Information and Power Transfer/Transmission) has become an attractive proposition as a viable method for powering Wireless Sensor Networks (WSN) or Internet of things (IoT) applications [7].

Therefore, the main motivation for the thesis is to take advantage of resources that were not previously available to generate energy, or that were not even considered as being capable of it [2]. This thesis is aimed to be a contribution for future research, as for the improvement of the amount of energy that can be harvested from the wireless power transfer. Besides, to deliver a research testbed capable to test any given waveform, such as meant for power transfer (WPT), for communications, and even for simultaneous wireless information and power transfer/transmission (SWIPT) systems.

## 1.2 Objectives And Scope

In current WPT using RF signals research, targets have been focused primarily in the improvement of individual elements in the power transmission chain, such as the rectifiers in the RF-to-DC converters plus the antennas obtaining the signal (rectenna). However, in recent years, the implementation and use of systems with feedback from the outputs to the transmitter (closed-loop) have been employed for improvement of the system as a whole [8]. Therefore, a research testbed with a closed-loop approach would be a promising acquirement for improving the total energy produce in WPT systems via RF.

The main objective of this thesis is to implement a testbed for RF power transfer using a Universal Software Radio Peripheral (USRP) Software-defined Radio (SDR) together with an energy harvester device. The general idea is illustrated in Fig. 1.1, where all main elements are shown and connected in a closed-loop system.

As seen in Fig. 1.1, the testbed scheme can be separated into the transmitter and the receiver side, with all their necessary elements for transmitting and acquiring the power of a signal. In the transmitter side, while the SDR transmits a signal the supplied power can be measured. Thus, the employed energy in the transmission of a waveform can be known. In the receiver structure, while the RF-to-DC converter obtains the transmitted signal and harvests energy, the analog-to-digital converter (ADC) delivers the harvested power as digital data (bits) to the microcontroller. Finally, a computer synchronizing and controlling the entire system is the central element in which the main program is executed.

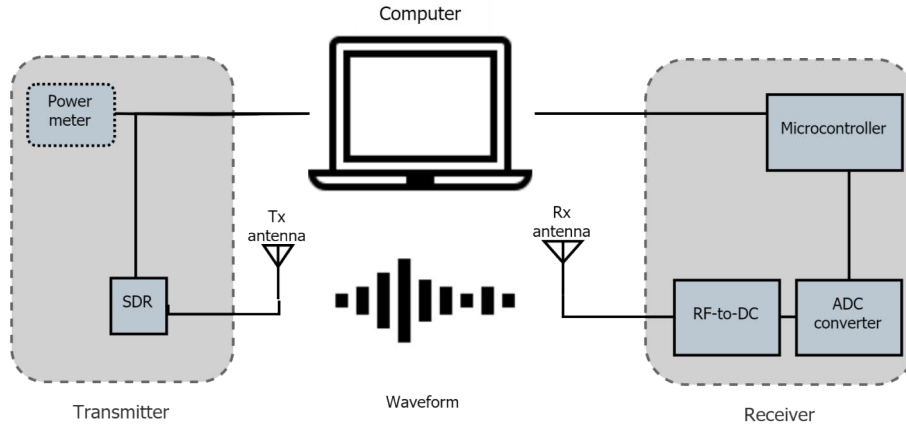


**Figure 1.1** The general project diagram, where the computer works as the central element. The computer controls and manages the transmitter side and process the data acquisition coming from the receiver. The power harvester together with analog-to-digital converter (ADC) and microcontroller are the testbed receiver side.

The main program is designed according to two functionality modes, the file transmission and the vector transmission. In the file transmission mode the testbed is capable to transmit any file containing a signal, or even more, a folder with many files. Similarly, in the vector transmission mode, a vector carrying a waveform within its elements is transmitted. The broadcast of a vector provides the possibility to perform an adaptive transmission for varying the elements of the vector, and consequently, obtaining different power harvested at the receiver. On other words, to transmit many times and in every transmission considering the resulted harvested power from the previous one.

The selected devices for the implementation of the testbed are; the universal software radio peripheral (USRP) NI2900 as the SDR, an ZY1273 USB power meter to measure supplied power, the P2110 and P1110 PowerCast® evaluation boards (EVB) as the RF-to-DC converters, the ADS1115 as the ADC, and Arduino Nano as the microcontroller.

### 1.3 Thesis Structure

The structure of the thesis consists of seven chapters as follows, the introduction of the thesis in Chapter 1, the literature review of the WPT field in Chapter 2, the theoretical background of digital communications in Chapter 3, the testbed structure with the considered devices in Chapter 4, the testbed functionality in Chapter 5, the operational assessments to test the implemented testbed in Chapter 6, and the conclusions of the thesis in Chapter 7.

The first chapter exposes the introduction of the thesis and its content is summarized in three sections, the background and motivation, the objective and scope considered, and the thesis structure.

The second chapter collects relevant information in current research in the WPT area and gives the literature review for the thesis. The Chapter 2 is ordered in three main sections, reviewing the wireless power transmission and focusing on the radio wave techniques, describing the current scenario in the RF WPT (Radio-Frequency WPT) research, and summarizing other testbed prototypes with similar approaches to the implemented testbed on this thesis.

The third chapter explains the theoretical background for understanding of the digital modulation and related subjects happening in the USRP transmission. Furthermore, Chapter 3 describes the theory behind the physical phenomena in the transmission of a signal through a medium.

In the fourth chapter are listed the considered devices for the implementation of the testbed, according to the structure where they are implemented. Besides, sections for the final hardware structure and the testbed software structure are also found in Chapter 4.

Chapter 5 works as a guideline of the functionality of the testbed, and is consisted of five sections. The functionality of the testbed starts with the setting of the parameters, the transmission modes (file or vector transmission mode), the program execution, and the obtained data once the execution of the system occurred.

Finally, Chapter 7 includes conclusion of this thesis, possible improvements and future developments in the testbed.

## 2. WIRELESS POWER TRANSFER

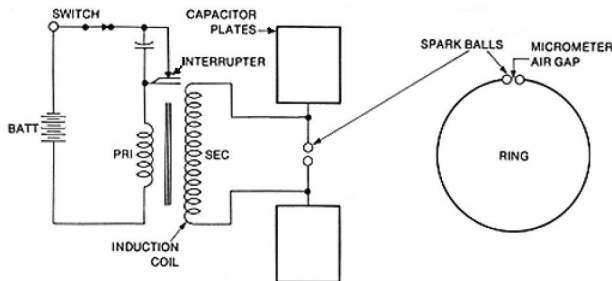
In this Chapter the literature review is found, and is ordered from the beginnings in the radio wave propagation of power to the current research in the WPT field through RF. Therefore, the scope of the chapter is narrowed down to WPT due to electromagnetic waves carrying energy.

This chapter has been organized into three main sections: radio wave power transmission, RF wireless power transfer systems, and WPT prototypes. Section 2.1 begins with a brief review about the history of wireless power propagation, and moves forward to MPT systems and their applications. In Section 2.2 is introduced the idea of obtaining energy from signals meant for communications and the challenges that this represents. Concluding, in Section 2.3 with a summary of current research implementing prototype testbeds with a similar approach to the deployed one in the thesis.

### 2.1 Radio Wave Power Transmission

Wireless power transfer (WPT) is a research topic that dates back more than a century ago when great inventors made experiments in the electromagnetic field. However, in recent years, the wireless transmission of power approach has come back even reaching to be an unmovable design feature in all upcoming wireless technologies, such as to energize devices in novel networks (e.g. wireless sensor network) [2,6].

As William C. Brown states in [11], everything began in the late 19<sup>th</sup> century with Heinrich Hertz's spark gap experiment [12]. The experiment of Hertz consists of the electromagnetic waves propagation in free space, which is the basis for wireless signal transmission [13]. As shown in Fig. 2.1(a), the device produces an induced current due to the electromagnetic waves spreading from the oscillator spark, and it generates sparks sending electromagnetic radiation into the gap. It was not until 1900 when Nikola Tesla started to carry out experiments related to power transmission, being the Wardencllyffe tower his most ambitious plan in 1904, as is shown



(a) Detailed schematics of the Heinrich Hertz spark gap Experiment, 1887 [9]



(b) Nikola Tesla's Wardencllyffe tower 1904. Located in the Long Island, New York [10].

**Figure 2.1** *Advances in electromagnetic waves had already started by the end of the 19<sup>th</sup> century. Heinrich Hertz changed the world with his spark gap experiment by proving electromagnetic theory (a). It was not until beginnings of the next century that Nikola Tesla designed his most ambitious energy transfer system with radio waves experiment, known as the Wardencllyffe tower (b).*

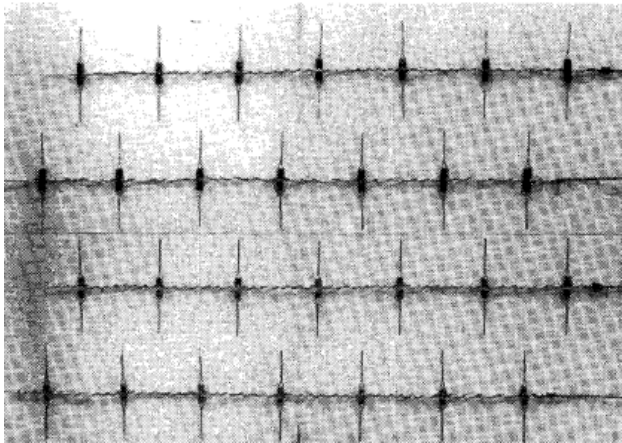
in Fig. 2.1(b). Tesla believed that by having many of these 56 meters high towers it would be feasible to have a power transmission network. However, when the first tower was almost completed, the funds for the project ended and it had to be dismantled [11].

More significant advances in the WPT field were made in the 1930's, with inventions such as the velocity-modulated-tube beam tube by O. Heil (also known as the Klystron tube) and the creation of the magnetron during the World War II by the British military forces [14]. Both devices can generate powerful microwave radiation, which are high frequency signals carrying energy.

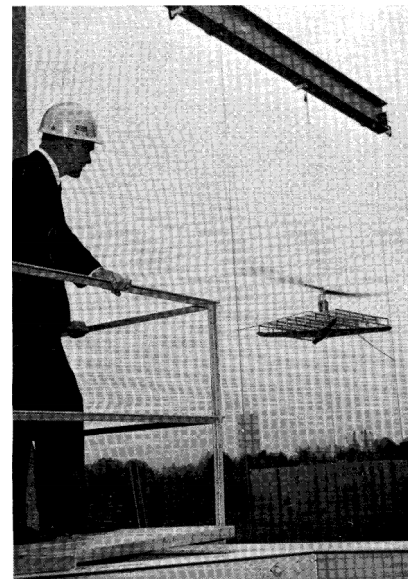
The next influential step occurred in the late 1950's and progress continued through the 1960's, in the research and advances achieved in the field of microwave power transmission. For example, in 1961 W.C. Brown conducted leading research into efficient power transmission without the need for intermediate cables [15]. In the same decade, details of the first rectenna prototype were published, as shown in Fig. 2.2(a). This was the result of a combination of half-dipoles antennas (28 in total) each with a rectifier made of semiconductor diodes [16].

Another interesting invention from the same era was a helicopter entirely powered by microwave energy, which used an improved version of the first rectenna proto-

type. The frequency for the microwave radiation was 2.45 GHz, which is within the bandwidths set aside for investigation and research purposes under the Industrial, Scientific, and Medical (ISM) range (2.4-2.5 GHz) [17]. In this ISM frequency range, the rectenna had the most efficient utilization of the microwave radiation [18]. The helicopter was constructed and tested in 1964 by Brown and others using more efficient diodes and a better diode array scheme [19]. The results of the trials were successful, as can be seen from the photograph in Fig. 2.2(b). Four years later, in 1968 Brown built an even smaller and more efficient rectenna using newer diodes, which could generate a maximum of 270 Watts, a great advance in comparison with the 7 Watts produced with the 1963 rectenna.



(a) First rectenna prototype [11], in 1963. It had 28 half-wave dipole antennas, each connected to a rectifier made of a semiconductor diode. The maximum output reached was 7 Watts, with an estimated efficiency of 40 percent.



(b) Microwave-powered helicopter during test, October 1964 [11].

**Figure 2.2** Significant advances in the field of MPT, with inventions such as the rectenna (a) and interesting approach to supplying energy over long distances using this technology, i.e. the microwave-powered helicopter (b).

The history of MPT is divided into two stages. The first stage was from the first experiments in power transmission (in 1886) with radio waves until the mid 1970's. After this point, the topic gain more interest, which meant more investment. For instance, one of the best-known pioneering organizations in the field was the National Aeronautics and Space Administration (NASA) [11, 20].

The most important milestones in the development of MPT are summarized in Table 2.1 [1], from the Hertz's spark gap experiment to the most recent advances, such

as the experiments conducted in Japan and other locations (Canada, Hawaii and France). It is thanks to these advances that wireless power transfer via radio waves (and more specifically MPT) has reached a certain degree of maturity. Furthermore, because the production and manufacture of electronic devices is now so much cheaper and more common that it was in the early years of this technology, it seems likely that WPT will feature more prominently in the future in the design of a number of devices such as sensor, and RFID tags, to name but a few.

**Table 2.1** Main WPT milestone in recent history [1].

Year	Milestone
1888	Experiments and demonstrations with electromagnetic wave propagation in free space, by Heinrich Hertz.
1899	First experiment on dedicated WPT, by Nicola Tesla.
1901	Wardenclyffe Tower project started by Nicola Tesla.
1964	Rectenna invention, by William C. Brown.
1964	Wireless powered tethered helicopter, by William C. Brown.
1968	Wireless powered beam-positioned helicopter, by William C. Brown.
1968	Solar power satellites idea proposed by Peter Glaser.
1975	54% achieved DC-to-DC power transfer efficiency in Raytheon Laboratory.
1975	WPT demonstration in JPL Goldstone, it achieved 30 kW DC transfer over 1.54 km distance.
1983	Rockets energized with WPT (MINIX project), a Japanese initiative.
1987	Flying-free wireless-powered aircraft experiments and demonstration in Canada.
1992	MILAX experiment with the phased array transmitter, conducted in Japan.
1993	ISY-METS wireless power experiment with rockets, conducted in Japan.
1995	ETHER experiment focused for powering airships with WPT, conducted in Japan.
1997	Project to transmit 10kW to a remote village, conducted in France.
2008	Successful WPT over 148km, conducted in Hawaii.
2015	Successful small device charging with power beaming, conducted in Japan.

The current scenario of technologies transmitting energy can be summarized in Table 2.2 [1], where MPT is part of the electromagnetic radiation. It is also seen that other three WPT technologies can be found, such as inductive coupling, magnetic resonant coupling, and laser power beaming. The main advantages and limitations, current and potential applications, and the representative companies are listed in Table 2.2 for every WPT main technology. Nevertheless, in this thesis the main focus is in the radiation of energy through electromagnetic waves.

**Table 2.2** Summary and comparison between WPT technologies [1].

WPT technology	Main devices	Typical range	Typical frequency	Main advantages and limitations	Current and potential applications	Representative companies
<b>Inductive coupling</b>	Wire coils	Millimeters to centimeters	Hz to MHz	High efficiency, require precise tx/rx coil alignment, very short range, single receiver only	Electric tooth brush and razor battery charging, transcutaneous charging of bio-medical implants, electrical vehicle charging, cell phone charging, factory automation	Powermat, Delphi, GetPowerPad, WildCharge, Primove
<b>Magnetic resonant coupling</b>	Tuned wire coils, lumped element resonators	A few meters, typically 4 to 10 times the coils diameter	kHz to MHz	High efficiency, safe, mid-range, large tx/rx size	Consumer electronics (e.g., cell phones, laptops, household robots) charging, biomedical implants charging, electrical vehicles charging, RFID, smart cards, industrial applications	PowerbyProxi, WiTricity, WiPower, Intel (Wireless Resonant Energy Link)
<b>EM radiation</b>	Dish antenna, antenna array, rectenna	Several meters to hundreds of kilometers	MHz to dozens of GHz	Long range, small receiver form factors, flexible in deployment and movement, support power multicasting, potential for SWIPT, LoS link is not a must, low efficiency, safety and health issues	Wireless sensor charging, IoT, RFID, consumer electronics charging, wireless-powered aircrafts, solar power satellite	Intel (WISP), Energos (Wattup), PowerCast, Ossia (Cota)
<b>Laser power beaming</b>	Laser emitter, photovoltaic receiver	up to kilometers	THz	Compact size, high energy concentration, no interference to existing communication systems or electronics, laser radiation is hazardous, require LoS link and accurate receiver targeting, vulnerable to atmospheric absorption and scattering by clouds, fog, and rain	Laser-powered unmanned airplane vehicle, laser-powered space elevator climbers, laser-based solar power satellite	LaserMotive

### 2.1.1 Microwave Power Transmission System

One approach to transmitting energy without cables is the use of microwaves, which are electromagnetic waves at high frequencies, specifically from 300 MHz to 300 GHz [21]. When talking about MPT it is important to make a distinction between the DC-powered microwave and information sent over these waves, MPT is pure DC transformed into microwaves [11, 22]. The MPT systems have the following main components, the microwave generator, the transmitting antenna, and the rectenna.

Figure 2.3 shows a practical wireless power system based on microwave transmission. On the transmitter side, a microwave source generates and sends radio waves carrying energy at high frequencies. In order to reduce the effects of outside interference, the radiated energy from the source goes through a coax-wave guide adapter, which in turn goes through a wave guide circulator [23]. Before the microwaves are sent through a medium (i.e. air) with an antenna, a tuner and directional coupler are needed to split and distribute the power of the signal. In the receiver side, the reverse procedure occurs, obtaining the transmitted signal with an antenna and transforming the microwaves into DC output. The rectenna is integrated with a low-pass filter for selection of the frequency to obtain, a matching network for purposes to match the impedance, and the rectifier which harvests the RF into DC.

The transmitters can be classified as microwave tubes, a microwave power module, and semiconductor microwave transmitter. The most widely used transmitter is the magnetron [11, 22], which is a microwave tube device. In the magnetron, the

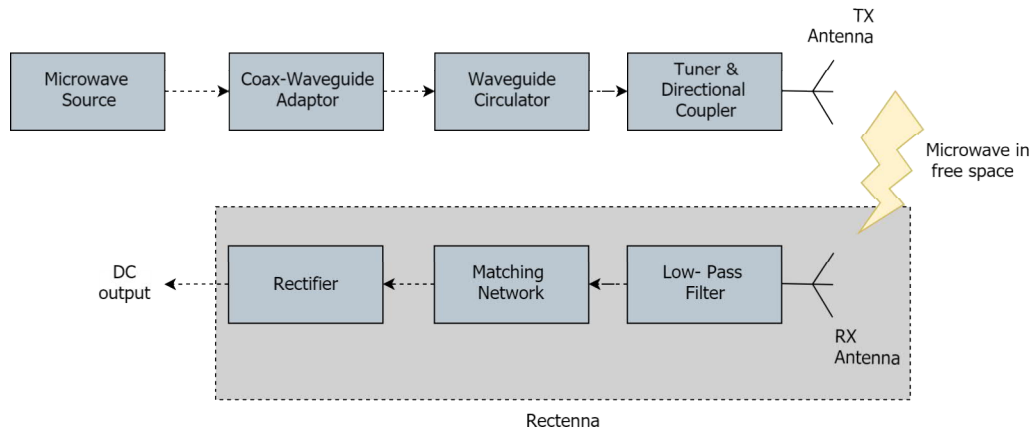


**Figure 2.3** A practical wireless power system based on microwave transmission. On the transmitter side are the power source and the electronics to control the output from the antenna, while on the receiver side the process is reversed. When the receiver obtains the microwave signal from the transmitter, it transforms the RF into DC through a rectifier.

microwave generation occurs between the interaction of electrons with a magnetic field. The magnetron has approximately 90% efficiency over the ISM bands commonly used (2.45 GHz) [24]. Research at other frequencies has also been performed, 8.5 GHz [25], 10 GHz [26] and even 35 GHz [24, 26].

There are different kinds of antennas for transmitting the microwave signals, the most used are the microstrip patch antenna, parabolic dish antenna and slotted wave guided antenna. The slotted wave guided antenna is a good option for power transmission as it has an aperture efficiency above 95 percent [22].

A rectenna is also essential for collecting the signal on the receiver side and being able to transform the RF to DC, which it does by processing them in a rectifier. Broadly speaking, the rectifier is compounded by diodes in which the obtained RF passes through and it is transformed in DC voltage. The diodes are used to only allow the flow of the electricity in one direction with a rectifying circuit, for example, it transforms an alternate current to a direct current [27]. The most widely used diode in current applications and research in MPT are Schottky diodes, due to its high efficiency, fast recovery time and low junction capacitance [28]. Furthermore, Table 2.3 shows the performance of a rectenna using different Schottky diodes in different frequencies and their measured efficiency compared with their calculated efficiency [29]. It can be noticed that the highest efficiency can be obtained at 2.45 GHz with a GaAs-W Schottky diode type, which is a diode made of gallium arsenide (GaAs).

**Table 2.3** Comparison for different diodes used in a rectenna.

Frequency (GHz)	Schottky diode	Measured efficiency (%)	Calculated efficiency (%)
2.45 [25]	GaAs-W	92.5	90.5
5.8 [30]	Si	82	78.3
8.51 [24]	GaAs	62.5	66.2

### 2.1.2 Microwave Power Transfer Applications

Numerous applications could benefit from the capacity to transfer energy without the need for power transmission cables [6]. Everyday technologies, such as the fast-growing market in RFID tags and electric vehicles all make use of this technology. There has recently been research into a design aimed for capturing and transmitting energy radiated from the Sun, and this technology is already in use by many of the satellites orbiting our planet [20].

One common application for MPT is with the radio frequency identification (RFID) tags, which have already been in use for decades. For instance, most large retail firms use RFIDs to identify and control losses due to pilfering and theft. Another common RFID application is the new "touch cards" which can transfer money just by being held close to a machine, thus obviating the need for pin codes or pushing buttons. As related in [5], it is shown that an RFID need not be a complicated system. On the contrary, it is the simplicity of the system which has helped make RFID tags part of our everyday lives. Besides, as they become more common, the costs of their manufacture have fallen rapidly over recent years.

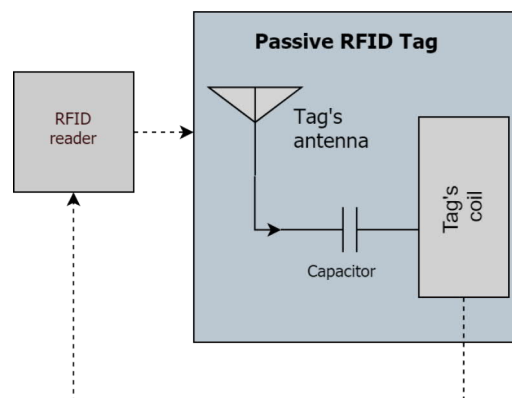


**Figure 2.4** Diagram for the RFID passive tags technology. The RFID tags are a MPT applications and due to its simplicity has become part of our everyday lives.

Briefly explaining the RFID technology, the system is compounded with two antennas as the transmitter and the receiver antenna, as shown in Fig. 2.4. The transmitter sends a signal and waits, until the RFID tag obtains and processes the signal for transmitting an answer as a response. The receiver side has a capacitor which stores the obtained energy from the RFID reader (transmitter), and when it is totally charged the capacitor supplies the voltage for running the coil of the tag. The coil of the tag will release a encoded radio wave containing specific information of the tag, the RFID reader obtains this encoded wave and is able to demodulate it [5].

In overall, tags are passive, which means that they do not have a battery on them. Therefore, the passive RFID tags operate with the energy from the transmitter (RFID reader). However, the disadvantage of not having a battery is that passive RFID tags operate in ranges of a few centimeters. On the other hand, active RFID tags including batteries are capable of higher frequency transmission with longer ranges (up to 100 meters) [5].

The MPT can be also employed for charging electric vehicles, being a viable solution to improve the long charging times for batteries [31]. For instance, in [32] a MPT system is proposed for charging an electrical vehicle, as seen in Fig. 2.5. As seen in the presented model in [32], the RF-to-DC process occurs at the roof of the electric vehicle, and the transmitter is directly transferring energy wirelessly to the rectenna.

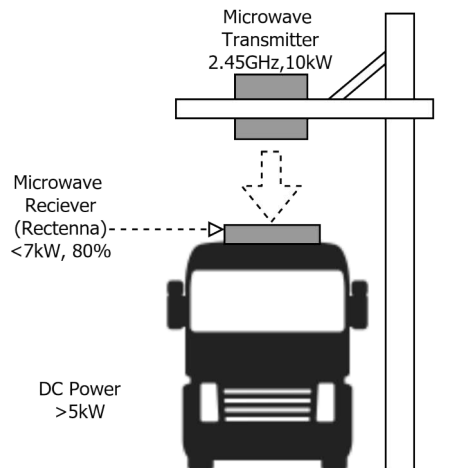


**Figure 2.5** A presented model in [32], it employs MPT wireless technology for charging an EV.

The outcomes of [32] indicate that from the transmitter to the receiver rectenna 80% is obtained, with a highly focused beam forming. Furthermore, the battery of

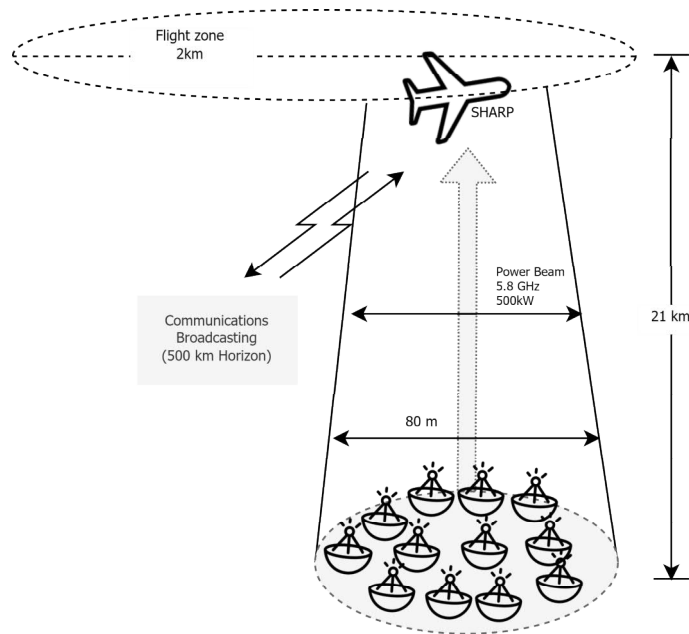


**Figure 2.6** Stationary High Altitude Relay Platform (SHARP) is unmanned airplane vehicle that can be used for communication relay purposes. The flying vehicle has a rectenna behind the wings, that transforms the microwave power to DC energy allowing long flight time.

the vehicle can get 5 kW, showing that MPT can be utilized for charging vehicles using electric motors.

A bigger scale of MPT application is the Stationary High Altitude Relay Platform (SHARP) [33], which is a unmanned airplane vehicle with a big attached rectenna on it. The plane can fly at about 21 km in height with a constant diameter (2 km) around transmitters on the surface of Earth. The flying vehicle can generate the power that needs to propel itself and achieve a long flight time, because its rectenna obtains the transferred MPT from the transmitters. As stated in [33], the long flight time and the obviating of a battery are the main reasons that makes SHARP an exceptional communication relay.

In Fig. 2.6 is shown the SHARP application diagram, which illustrates the maximum height and the diameter of the flight zone that the flying vehicle can reach, 21 km and 2 km respectively. The transmitter antennas deliver the energy as a power beam (microwave radiation) with 5.8 GHz frequency carrying 500 kW. It is also seen in the diagram the 500 km horizon that the flying vehicle can achieve for communication broadcasting.

The approach to transmit energy in long distances has encouraged the use of MPT technology for harvesting solar energy in satellites orbiting Earth. The solar power satellites is an ambitious concept that started at the end of the 1960's [1], and its

primary plan is to take advantage of the almost unlimited solar radiation resource in the atmosphere [20].

The solar power satellite system harvests the radiation from the Sun in satellites and transmits (DC-to-RF) with a microwave beam the energy to receivers in the surface on Earth, as shown in Fig. 2.7. The receiver station on Earth transform the microwave beam in DC energy (RF-to-DC) which is integrated into the power grid.

The system can obtain higher harvested power from the Sun in comparison with other renewable sources on Earth surface. For instance, in [20] is explained that while solar radiation in the capital of Japan (Tokyo) is approximately  $140 \text{ W/m}^2$  on average along a year, a geosynchronous satellite orbiting Earth gives a constant  $1400 \text{ W/m}^2$ . Therefore, the difference between a solar panel on Earth against a solar power satellites is around 10 times more.

There are still many challenges to face for implementing a system using satellites, such as the improvement of the efficiency between radiated energy to DC, which it is believed that could achieve over 80% in the near future [20]. Also, the attenuation due to atmospheric conditions and in the ionosphere can affect the microwave signals. Besides, the extreme long ranges for transmission creates an essential challenge for accuracy acquisition of the microwave beam at the rectennas. According to [20], it is expected about 12 years from now to have a network of satellites harvesting energy from the Sun and feeding electricity in the electric grid, due to the current research scenario to confront the problems related to the system.

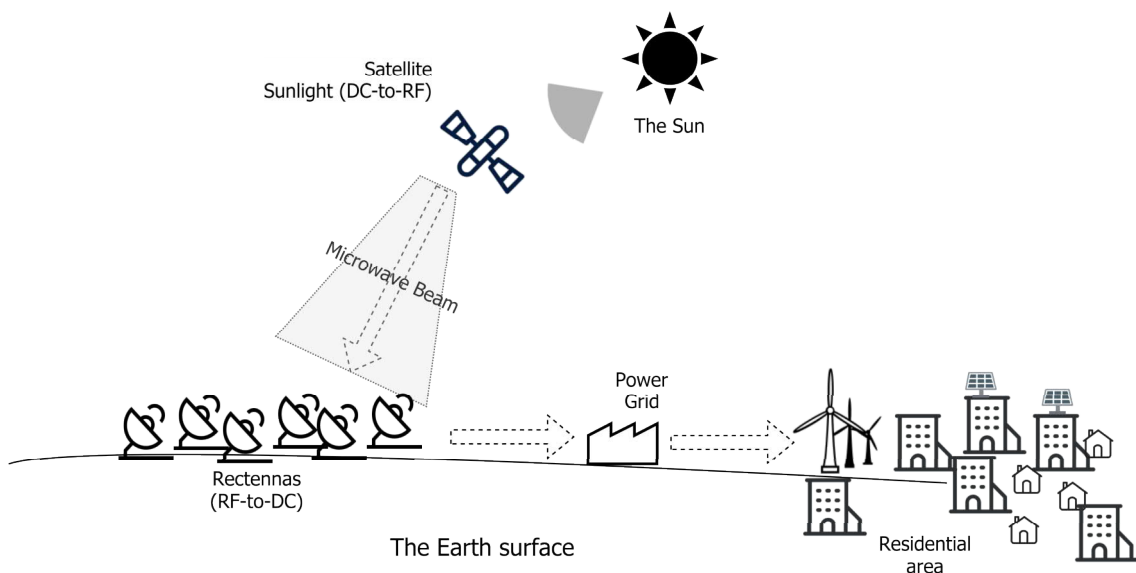


**Figure 2.7** A Solar power satellite system where a satellite is transforming solar radiation into DC and then transmitting the energy as a microwave beam to Earth, where rectennas do the reverse operation to add the obtained energy into the power grid. [20]

## 2.2 RF Wireless Power Transfer Systems

The successful adoption of devices and methods for transmitting power wirelessly by the market (i.e. the RFID tags and mobile phones charging wirelessly on docks) has opened the door for newer possibilities. An interesting research field is to use available resources for energizing devices, such as the RF signals that cellular networks are continuously delivering [6].

The attenuation on wireless propagation has contained the power transmission through RF signals (as in communications) mainly in short distance ranges. Nevertheless, the WPT through RF signals still is an attractive solution and a viable method for future advances such as powering wireless sensor networks (WSN) or internet of things (IoT) applications, because of the upcoming reduction of propagation losses thanks to the 5<sup>th</sup> generation of cellular networks, small cell networks and enhanced multiple-input multiple-output (MIMO) systems [7].

Wireless power transfer via RF can be separated in two, one assuming exclusively power transmission from the transmitter, and the other method considering to harvest energy from dedicated communication signals, they are called wireless energy harvesting (WEH) and wireless power transfer (WPT) respectively [34].

The recent increase in the research of WPT through RF is supported due to the constant improvement in the amount of required energy in a fixed computer load. For example, at the speed at which the information technology evolves, the necessary power decreases by a factor of two approximately every 1.2 years [35]. The integrated circuits are becoming more focused on efficiency, such as ultra-low power devices considered in upcoming applications (i.e. WSN and IoT) [36]. The decrease in the needed power that devices are aiming makes possible a low-power delivery by WEH and WPT, values from micro watts to few watts in short and long ranges [37, 38]. Besides, the power delivery is not only limited for low-power devices (e.g. RFID tags and sensors), but also for personal electronic devices as computers and mobile phones [39, 40].

In addition, the growing interest in WPT through RF signals has brought together different companies and organizations to investigate and find new solutions in the area [34]. For instance, since 2013 in Europe exist the COST IC1301, a cooperation between countries for study and research purposes in the area of wireless energy transmission [39].

### 2.2.1 Requirements And Challenges For A Power Network

The new opportunities that a wireless power network opens are several [4]. In the first place, it permits true mobility by decentralizing the power source, which allows devices to be genuinely independent. Secondly, the batteries of the devices will reduce their size and even to the point of being unnecessary for some applications, such as low power sensors. Third, the design of smaller and lighter devices could be a real possibility [34].

The current cellular network in which cell phones and other devices operate is exclusively for communications purposes (information/data transfer). While a new power network is not yet in the first generation, the modern mobile communications network is about to reach the fifth generation (5G). In addition to the regulation for human exposure to electromagnetic fields (as in MPT), there are no standards related to mobile power [34].

The transmission of energy and information through radio waves has always been considered as two different branches of research. As a consequence, both technologies evolved separately and generated two main challenges for the current scenario, the modern wireless network is continuously transmitting RF for communications purposes but not energizing devices, and for achieving a wireless power network it is necessary to change or even redesign everything in the mobile network with energy transmitters.

The main challenges for designing a network in which power and information transmission occur are particularly with the transmitter-receiver relation, the signal design, and the network architecture. In addition, the efficiency of the energy transaction must be increased (from end-to-end), in cases of line of sight (LOS) and without line of sight (NLOS) with the receiver moving at different speeds. The accessibility of power has to be equal and constant in the whole network, adding regulation related to health and safety for RF radiation. Thus, to have control over the distribution of energy towards the covered devices must be taken into account [2, 4, 34, 38].

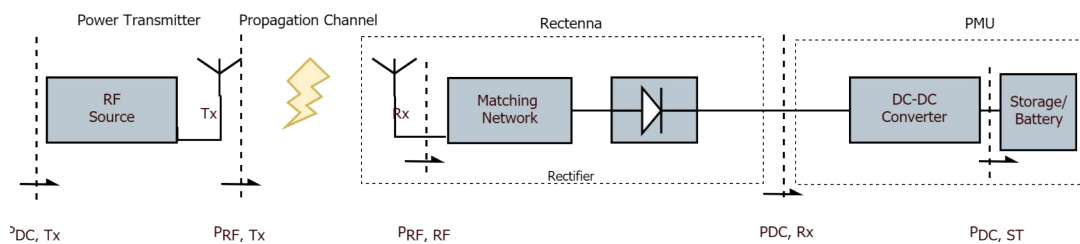


**Figure 2.8** Block diagram for a general far-field WPT transmission. In the diagram it is possible to observe the different stages of the overall system efficiency " $e$ " (end-to-end).

### 2.2.2 Design For Far-Field RF WPT System

The general design for a far-field WPT system using RF signals can be summarized into three primary components, such as the power transmitter, the rectenna, and the power manager unit (PMU), as seen in Fig. 2.8.

The power transmitter is integrated with the RF source, which produces the signal that is going to be sent in the transmitter antenna (Tx). After the transmitted signal goes through the propagation channel is received in the rectenna block. The rectenna block is composed of the receiver antenna for the acquisition of the signal, the matching network block for matching the impedance at the rectifier, and the rectifier to transform the received RF in DC energy. Finally, the harvested energy from the rectenna stage is stored in the PMU block (i.e. in batteries).

The end-to-end efficiency ( $e$ ) of the system shown in Fig. 2.8 can be calculated as the ratio between the transmitted power and the harvested energy at the output, as presented in equation 2.1. Thus, the total efficiency between the transmitted DC and the stored DC can be calculated as  $\frac{P_{DC,ST}}{P_{DC,Tx}}$ .

Furthermore, the total efficiency ratio ( $e$ ) can be separated according to the general design for a far-field WPT system using RF signals into four stages. The ratio between the converted DC energy to RF in the power transmitter stage can be calculated as  $\frac{P_{RF,Tx}}{P_{DC,Tx}}$ . In the rectenna stage, the ratio between the obtained RF with the transmitted RF in the transmitter is  $\frac{P_{RF,Rx}}{P_{RF,Tx}}$ . After the rectifier in the rectenna stage, the ratio between the rectified DC with the received RF at the rectenna is  $\frac{P_{DC,Rx}}{P_{RF,Rx}}$ . In the PMU stage, the ratio between the stored DC and the rectified DC can be calculated as  $\frac{P_{DC,ST}}{P_{DC,Rx}}$ .

Therefore, the overall efficiency of a far-field WPT system ( $e$ ) can be enhanced by improving any of its four ratios ( $e_1$ ,  $e_2$ ,  $e_3$  and  $e_4$ ). Consequently, the control over the efficiency system can be achieved. In [7] the research related to the measurement of the power of GSM900 base stations shows that the best approach to control the efficiency of the system is in WPT systems, in comparison with WEH. Concluding that, the WPT systems can be optimized entirely and diverse methods can be employed for improvement of the overall efficiency or its separated sections.

$$e = \frac{P_{DC,ST}}{P_{DC,Tx}} = \underbrace{\frac{P_{RF,Tx}}{P_{DC,Tx}}}_{e_1} \underbrace{\frac{P_{RF,Rx}}{P_{RF,Tx}}}_{e_2} \underbrace{\frac{P_{DC,Rx}}{P_{RF,Rx}}}_{e_3} \underbrace{\frac{P_{DC,ST}}{P_{DC,Rx}}}_{e_4}, \quad (2.1)$$

**DC To RF At Power Transmitter ( $e_1$ )**

The efficiency of a WPT system can be improved in the RF source by increasing the transmitted power. One method to optimize the efficiency between DC and the RF conversion is using power amplifiers, which can generate more power from the RF source by boosting the gain at the output [4].

Power amplifier designs that take into consideration the nonlinearities and harmonics can boost and achieve better output power at the transmitter, compared when no amplification is employed. Additionally, amplification with a restricted PAPR (peak-to-average power ratio) in WPT systems proved to be beneficial for the increment of the efficiency  $e_1$  [41]. More details on non-linearities, power amplification, and PAPR are in Chapter 3.

**RF To RF At Receiver side ( $e_2$ )**

The RF to RF efficiency on the receiver side can be improved with the use of directional transmission. With a more accurate power transmission in the transmitter, the rectenna in the receiver can obtain a better percentage of the transmitted power.

The current research for improving  $e_2$  is focused on real time systems that reconfigure the transmitted array based on the location of the receivers, the phase of the array, and retro directive arrays using phase-conjugations methods [42–44]. In addition, the equivalent isotropically radiated power (EIRP) regulations for WPT systems are needed [34].

**RF To DC At Rectenna ( $e_3$ )**

The efficiency  $e_3$  can be maximized by using rectennas with high conversion efficiency. In order to improve the efficiency at the rectenna, the rectification of the RF signal arriving from the transmitter to DC energy must be increased.

The design of efficient rectennas can be achieved by optimizing them according to a specific frequency and power input. On the other hand, in WEH systems the improvement of  $e_3$  is more complicated, due to the wide input power range and different spectra of the approach [45]. An example to improve the efficiency of a rectenna is the use of broadband frequency techniques, where frequencies of narrowbands are selected for different rectifiers [46].

Furthermore,  $e_3$  not only depends in the rectenna design, it also relies in the input waveform and modulation. Such as, the proper selection of the waveform for WPT proves that rectifiers are able to generate more energy at low input power [27, 47–50].

### DC To DC At Power Management Unit ( $e_4$ )

The DC to DC conversion relies mainly in the matching network block in the far-field WPT diagram, as shown in Fig. 2.8. The rectenna load variability is the main challenge to face for improvement in the efficiency  $e_4$ .

The matching between rectifier and load can be complicated due to several elements, such as the variable diode impedance for different power levels, the rectifier input is variable, and the rectifier nonlinearities at the output. One method to maximize the  $e_4$  efficiency is to track the rectifier maximum load (optimized matching), as in [51, 52], where DC to DC switching converters were used to find the maximum power. For instance, in case of multisine waveforms, the most efficient scenario is with an optimized matching [53].

### Efficiency Of The System, End-to-End ( $e$ )

The total end-to-end efficiency can be maximized by enhancing every zone of the far-field WPT diagram (Fig. 2.8). However, it must be taken into account that elements related to the improvement of one sector have repercussions on others. For example, a transmitted signal affecting the efficiency  $e_1$ , and its associated power improving the rectified energy in  $e_3$  [34]. Therefore, it is essential to consider all four when trying to find the best optimization of the system [34].

In spite of experiments with closed-circuit systems (i.e. [54]), the WPT design has been mainly centered on opened-loop methods (as in Fig. 2.8). The opened-loop approach can not obtain the channel state information (CSI) because of the lack of a feedback from the receiver side to the RF source, so the system output is not considered for transmission purposes [6].

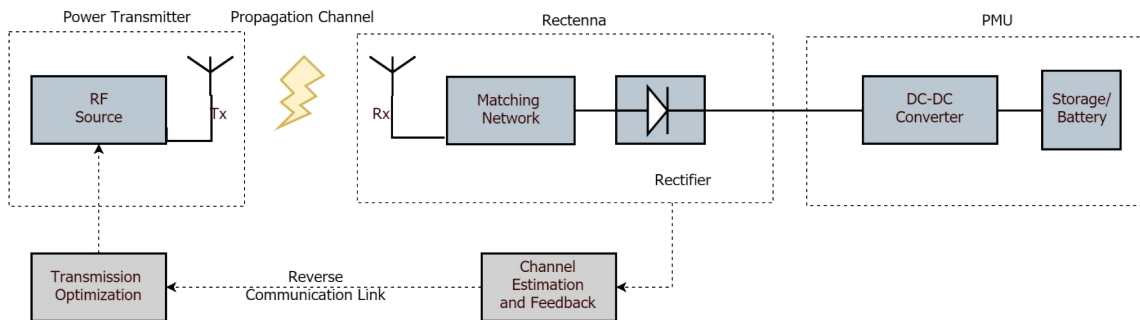
### Improved Closed-Loop RF WPT Design

Figure 2.9 presents an adaptive far-field WPT architecture, which has the same blocks as in Fig. 2.8, but a channel estimation and transmission optimization block

are added creating a closed-loop transmission. Thus, the system becomes more automated, even without the need for human intervention to change the parameters in the transmitter.

The reverse communication link facilitates a feedback from the receiver to transmitter, by the channel estimation and feedback block. Therefore, the transmitter can use useful information that could help to improve subsequent transmissions. For instance, if the transmitter has CSI, it is possible to suitable adapt more power delivery in frequencies not so attenuated by the propagation channel. Furthermore, if there is a MIMO scenario, transmitters would be able to adapt the power sent by taking into account that the receiver is obtaining power for more participants.

The transmission optimization block would improve the beamforming and waveform design at the transmitter with the feedback information. This improvement would maximize the efficient between RF to DC conversion ( $e_2$  and  $e_3$ ). For example, changing transmitted power and the PAPR related to the waveform design. Therefore, these elements of the feedback must be integrated in the signal design, creating a systematic design methodology [34].



*Figure 2.9 Architecture for an improved far-field WPT transmission.*

### 2.2.3 WPT Signal And System Design

Along with the research in the RF WPT system design, current work in the signal design related to power delivery wirelessly is conducted. For instance, in [1], where the design of useful elements in the transmitted signal, CSI, MIMO strategies, WPT together with information delivery are gathered and reviewed.

In [8, 55], a closed-loop design is taken into account. The simulated work reveals that it is possible to improve the signal transmission with a system that can handle collectively the power allocation, the waveform design, and the beamforming of the broadcast. Besides, the optimization of the transmitted signal can be done (at the

power transmitter) by using the obtained CSI from the reverse communication link combined to an adaptive PAPR. Additionally, in the closed-loop design in [48, 56], the beamforming gain, the frequency diversity gain, and the nonlinearities of the rectenna with Taylor models are maximized.

As expected in the WPT closed-loop system in [8, 55], by taking into account the nonlinearities, the adaptive and optimized multisine signals show a better efficiency compared when no adaptation is done in multisine signals used in [27, 47–49]. In addition, the power transfer is improved when the power allocation is used at frequencies with more gain and less power allocation at those frequencies with greater attenuation of the channel.

In [8, 55] is also demonstrated that a frequency diversity gain can be acquired with a waveform adapted by the frequency response of the channel and multipath propagation. Even more, [8] demonstrates that an increase in the signal PAPR is not a correct approach for WPT design, as claimed in [49, 50]. Although high PAPR signals in a frequency-flat channel work for improvement in the obtained DC at receiver, it is not valid in multipath and frequency selectivity cases.

In contrast with the theory, in a practical application, the transmitter does not have entire knowledge of the CSI. Besides the reverse link between the power transmitter and the receiver, techniques to obtain the CSI must be adopted. Thus, three methods are considered, the forward link training with CSI feedback, the reverse link training with channel reciprocity, and the power probing with limited feedback [1, 34].

According to [57], the first two techniques aforementioned are highly comparable with the adopted ones in the current communications systems; the forward link training with CSI feedback, and the reverse link training with channel reciprocity. However, these two techniques are not the best approaches for WPT, as stated in [58] where the power probing procedure is used by having one bit per feedback interval which indicates the state of the harvested power (increase or decrease). The power probing technique raised as the best approach for WPT, due to its implementation requires low communication and signal processing at the terminal [34]. Furthermore, the power probing with limited feedback depends on the output DC from the rectenna and a defined number of bits used for feedback.

The power probing with limited feedback in turn can be separated into two methods for the CSI acquisition as in [59], the waveform selection and the refinement strategy. The waveform selection mode transmits through several pre-coded time slots, which the transmitter and the receiver know from beforehand. Once the signal is

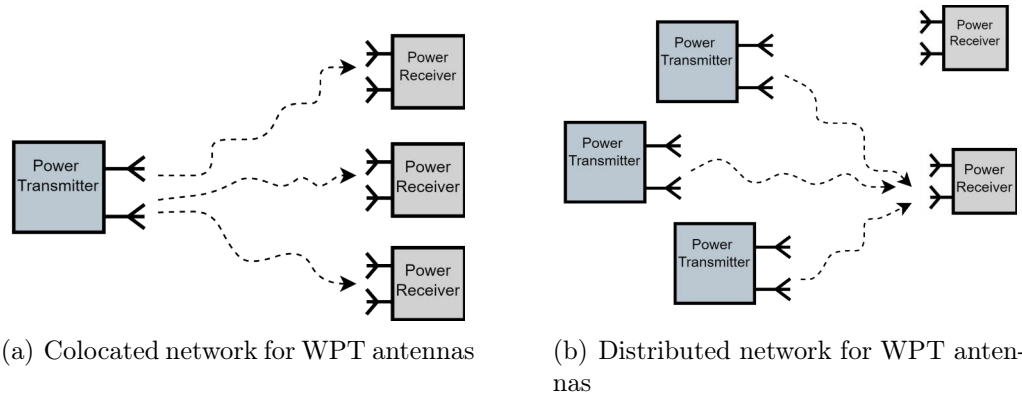


**Figure 2.10** Two proposed WPT network for allocation for multiple receiver and transmitter antennas, colocated network (a) and distributed network (b).

received, the receiver sends a limited bit feedback with the index of the largest harvested energy slot. The second method, the waveform refinement, is a strategy that transmits two consecutive waveforms in different stages, then the receiver returns one bit to the transmitter telling if the harvested power increase or decrease.

So far, it has been considered one-to-one transfer of energy. Nevertheless, WPT systems are not limited to this scheme. As [8, 60], which propose different design schemes for a WPT with RF signals in a multi-user scenario. Briefly explained, there is a dependency between the harvested energy generated by the rectennas. For instance, all rectennas having different performances with the same waveform produce that the provided power varies for every user. Thus, in a multi-user scheme, the compensation between users must be considered.

There are two main scenarios for a multi-user network analogous to the current communication network, the receivers harvesting power from multiple transmitted signals (colocated antennas), and a defined number of transmitters for a specific receiver (distributed antennas) [34]. As shown in Fig. 2.10, where in a colocated network (Fig. 2.10(a)) a transmitter delivers power to all receivers available, and in a distributed network with multiple transmitters only transferring power to one receiver (Fig. 2.10(b)).

The research proves that cooperating antennas transmitting energy in a distributed system is a more suitable solution for an ubiquitous coverage [1]. To mutually transmit power to specific receivers the right approach for wireless power delivery across the network is a distributed network as in Fig. 2.10(b), and at the same time avoiding energy beams detrimental for people [34].

### 2.2.4 Wireless Power And Wireless Information Integration

A mobile network in which both the transmission of information and the transfer of energy are integrated is the main objective of the current research in the area. A wireless information and power transfer/transmission (WIPT) network would integrate both paradigms, for transmitting data and power to the final user. According to [4,34], the WIPT can be classified into three main methodologies, simultaneous WIPT (SWIPT), wirelessly powered communication network and Wireless powered back-scatter communication (WPBC).

- In a SWIPT configuration, energy and information occur at the same time. Both arriving simultaneously in the down-link at the receiver (or several receivers), by using one or more access point. It is also possible that the energy receiver and information receiver are part of the same device or both being different devices. For example, a cell phone charges and obtains information at down-link. On the other hand, a low-power device attached to the cell phone obtains the power transmitted, and at the same time the cell phone receives the data in the down-link [4].
- In a wirelessly powered communication network, both down-link and up-link are applied alternately, for power and information transmission respectively. For instance, a low-powered device harvests the energy from the transmitter and utilizes it to send information in the up-link [4].
- The wirelessly powered back-scatter communication (WPBC) approach is similar to the previous one using down-link for energy transfer. However, a back-scatter tag sends modulated information back to the transmitter in the up-link [2].

Transmission strategies must be conducted for characterization of the trade-off between power and communication in WIPT, such as a signal that maximized the DC output at the rectenna does not maximize the rate as well. In [61], a simultaneous broadcast is performed with frequency selectivity technique, where a channel with multiple sub-bands is employed. The conveyed power is raised by transferring all the energy in sub-bands with better performance (the strongest ones in the frequency domain), leading to more DC output from the receiver rectenna. However, the approaching the energy does not increase the rate. In case for increasing the rate, a transversely information in various sub-bands and with water-filling algorithm allocating power through the sub-bands can be conducted [62]. Therefore,

the transmitter has to control the trade-off between rate and power, deciding the power allocation through the sub-bands for certain rate levels.

On the other hand, at the receiver side, with a defined architecture the trade-off between rate and energy can be improved [63]. One approach is to establish time slots for data acquisition and energy harvesting, which leads to incorporate an information decoder and a PMU with a rectenna at the receiver. Thus, the transmission block at the transmitter can be divided into two orthogonal time slots, one for data, and the other for power transmission. In both divided time slots the data is maximized and the energy waveform optimized, then the receiver changes between data acquisition and energy harvesting sporadically. The duration of the alternative changes in the time intervals can be controlled in the receiver, producing different trade-offs between the energy and the acquired data.

## 2.3 WPT Prototypes In The Literature

Numerous prototypes and testbed implementations that are related to the testbed created in this thesis are found in the literature. In this section, relevant designs and their results are presented and described. First, the first closed-loop testbed implementation found in literature and its results are presented. Then, testbed prototypes implemented for several application found in the literature are listed and summarized.

In [54], the first closed-loop WPT system for dynamic CSI acquisition and adaptive waveform optimization is performed. The system works at 2.4 GHz with 5 meters distance between transmitter and receiver. For purposes to obtain feedback and to optimize the waveform according to the channel, an SDR in the transmitter side is required. At the receiver side, a manufactured rectenna with a Schottky diode transforms the obtained RF in DC power.

The results of [54] concludes that a systematic waveform design must integrate the diode nonlinearity to improve the WPT performance, and also to take into account the propagation channel effects, proving the simulated results of [8,64]. The results also show that in frequency selective channels scenarios the CSI and channel adaptive waveforms are fundamental to raise the performance (such as in NLOS). The research concluded that, the channel frequency diversity gain is beneficial for larger bandwidths and in frequency selective channels the waveform PAPR is not a reliable metric to evaluate optimization.

Furthermore, the implemented testbeds for WPT research are in several applica-

**Table 2.4** Summary of implemented prototypes in RF WPT research

Field of research	Prototypes	Main characteristics
WSN	[65]	P2110 EVB as the receiver, and WPT in 915 MHz band.
	[66]	P2110 EVB as the receiver and TX91501 for transmission. WPT frequency at 915 MHz.
IoT	[67]	P2110 EVB as the receiver and USRP N210 for transmission. WPT frequency at 915 MHz.
	[68]	P2110 EVB as the receiver and 21 USRPs (N210) for transmission.
Ubiquitous and directional power delivery	[69]	Rechargeable node sensor connected with a P2110 EVB in the receiver side, and TX91501 for transmission. WPT frequency at 915 MHz.
	[70]	Rechargeable node sensor connected with a P2110 EVB in the receiver side, and TX91501 for transmission. WPT frequency at 915 MHz.
Multi-source harvesting	[71]	P2210 EVB together with a solar panel and a thermal harvesters. WPT frequency at 915 MHz.

tions. Such as, wireless sensor networks (WSN) [65, 66], internet of things [67, 68], ubiquitous and directional power delivery [69, 70], and power harvesting from multiples source [71]. Most of them use similar devices, if not the same, as the employed ones in this thesis. Table 2.4 summarizes the main components of every reviewed testbed in this section.

Two protocols for WSN are proposed in [66], focused in scheduling. These protocols are for the configuration of the activity of the chargers, one oriented to the load charging and the other oriented to the energy balance. In the first case, the protocol relies upon the charging efficiency. In the second protocol, the configuration is based on the fact that all the chargers in the system have the same energy reserves. In [66], both protocols are simulated and compared with the performance in a implemented testbed, which is integrated with transmitters and RF to DC converters built by the PowerCast company (TX91501 and P21110 EVB respectively). The energy harvesters deliver power to wireless sensors that are communicating to each other every 50 ms. The results of the research expose that, in both protocols their primary goal are accomplished, such as an improved charging efficiency in the charging oriented protocol, and a uniformed energy distribution between chargers in energy balancing protocol. Finally, [66] concludes the possibility to have a trade-off between the two models in mobile chargers.

In case to energize IoT devices, there are two recent research in the field, both with different approaches but with interesting results [67, 68]. In both research, the PowerCast P2110 EVB and Universal Software Radio Peripheral (USRP) model N210 are employed. The first method [67] is an iterative adaptive technique to maximize the beamforming signal in a far-field WPT transmission. The receiver side includes a rectifier that converts RF to DC and also gives feedback of the received signal strength indicator (RSSI) for forwarding adaptive improvement in the beamforming with the blind adaptive beamforming algorithm (BABF) strategy. The results prove the improvement of the beamforming signal with BABF, in comparison when no using the adaptive strategy. The testbed was used in the ranges between 50 cm to 1.5 m with a multiple input single output (MISO) scheme, up to four transmitter antennas and one receiver.

The second strategy for powering IoT devices is to have an area of coverage and delivering energy for any device within, employing a distributed beamforming. In [68] is implemented the Energy Ball model, which can achieve asymmetrically energy transmission. In other words, while the system increases the energy density for a specific device inside the area, other areas have low-density energy. The results reveal that for a  $20 \times 20 \times 30 \text{ m}^3$  area with 21 distributed USRP transmitters, it is possible to transfer over 0.6 mW of RF power within the range, when using the developed model.

In addition, one of the first research proposing an omnidirectional chargeability with directional antennas is found in [69], and it is improved into the use of directional antennas charging a wireless charger within an area in [70]. In both directional antennas research, a theoretical model is developed and put into a testbed for experimental results. In the practical experiments, the transmitters and the receivers are PowerCast company devices (TX91501 and P21110 EVB respectively).

In [69], the research shows a implemented model for directional charging between chargers and devices, an efficient technique to check omnidirectional chargers in an area, and a derived upper bound for a random deployment charging probability. The results from the experiments show an improvement of the coverage detection in comparison with algorithms in the WSN literature (i.e., full-view coverage [72]).

On the other hand, in [70], placement with optimized charging utility (PLOT) model is implemented for a uniformly distribution of devices receiving energy from a fixed number of chargers optimizing the charging utility of the system. The research and experimentation conclude that field tests prove the developed algorithm for an empirical directional charging model.

Apart from the pursuit of WPT systems using mainly RF radiation, conducted research to integrate this technique with other energy source methods are in the current investigation. For instance, in [71], where a multi-source procedure to harvest energy is developed. The main objective is to create a robust system in which several harvesting systems are tested separately and compared with the unified method, in which all systems are in a parallel connection feeding a capacitor (storage). The selected energy sources are solar and thermal, and also the RF radiation from a transmitter. In the case of RF to DC conversion a P2110 EVB is used, a solar energy harvesting panel for solar energy, and a thermal energy harvesting system for the thermal source. The results in [71] reveal that a multi-source power harvesting produces more energy than every method for separated.

### 3. DIGITAL COMMUNICATIONS

All modern communications are mostly based on the digital transmission of discrete values, i.e. bits. In turn, digital communication is based on analog carrier signals that carry encrypted information on them. Thus, due to the analog and continuous performance of the carrier signal, digital communication is under physical limitations in the transmission. For example, the bandwidth and the power associated with the transmitted waveform.

The overall chain of digital communication (Fig. 3.1) has at least four functionalities: The source coding/decoding, the channel coding/decoding, the modulation/demodulation, and the propagation channel [73]. The source coding/decoding is in charge to generate the digits that represent the message (bits), they must be as few as possible without redundancy. Once a digital representation is completed, controlled redundancy can be done for purposes of error control coding at the receiver side (channel coding/decoding). After the signal is obtained as an analog waveform at the receiver (modulated signal), a correct conversion into digital information is followed (demodulation). However, the transmitted and the received signals are not the same because the transmission happens in a physical channel where noise, interference, and distortion are always affecting the signal.

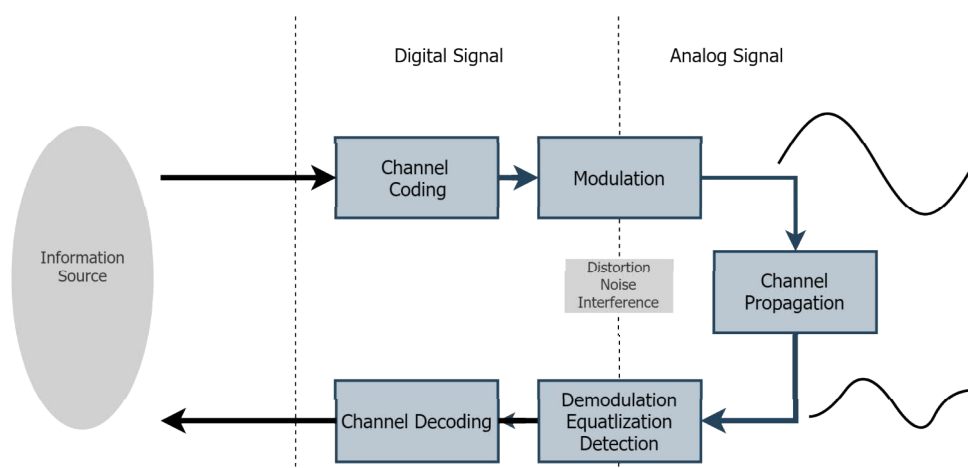


**Figure 3.1** Basic diagram for a digital communication transmission with its primary blocks.

This theoretical framework describes the phenomena that occur in the transmission from the SDR until the reception in the receiver side. Because, at the rectenna, there is neither decoding nor demodulation of the transmitted signal, this chapter is focused on the digital processes at the transmitter and at the channel. Section 3.1 explains a complex modulation (I/Q, in-phase and quadrature). The section 3.2 summarizes the OFDM multicarrier technique and related subjects. Finally, Section 3.3 ends with a summary of power amplification of the signal and how it produces non desired elements such as nonlinearity and harmonics.

### 3.1 I/Q Modulation And Constellation Representation

One technique in digital communication is to modulate the signal with their quadrature and in-phase component, the I/Q modulation. As seen in Eq. 3.1, the in-phase and quadrature modulation is based that a sine wave can be represented with its angular frequency ( $w = 2\pi f$ ), phase( $phi$ ) and amplitude ( $A$ ) components. According to trigonometry, a sine wave can be separated into a component (in-phase) in the real axis of a Cartesian plane, and a component in the imaginary axis (quadrature). After replacing with trigonometric identities in Eq. 3.1 by taking the addition between the frequency ( $w$ ) and the phase ( $\phi$ ) inside the cosine as a subtraction of a cosine and sine wave, Eq. 3.2 is obtained [74].

$$x(t) = A(t)\cos(\omega t + \phi(t)) \quad (3.1)$$

$$x(t) = x_i(t) \cos(\omega t) - x_q(t) \sin(\omega t) \quad (3.2)$$

$$x(t) = \text{Re}[x_{I/Q}(t)e^{j\omega t}] \quad (3.3)$$

Therefore, the wave can be modulated by separated according to its in-phase and quadrature components, by increasing the  $x_i$  or the  $x_q$  amplitude respectively (Eq. 3.2). The changes on the amplitude of the I or Q elements of the signal will generate variations for the amplitude, the frequency, and the phase, making the implementation of a signal modulator simpler, because it is not necessary to vary the phase of a RF sine wave carrier directly [75].

Figure 3.2 shows a general block diagram for an I/Q signal modulator, where D/A block transforms the digital signal (bits) into an analog one, the LPF block representing the low-pass filter, and the mixers where the I and Q components get up-converted (or down-converted) by the carrier frequency of the system. Both branches are multiplied by the same sine wave (carrier) but with dis-phase of 90

degrees, therefore, in Fig. 3.2 at the mixers are cosine and sine function with the same angular frequency ( $w_c$ ) [76].

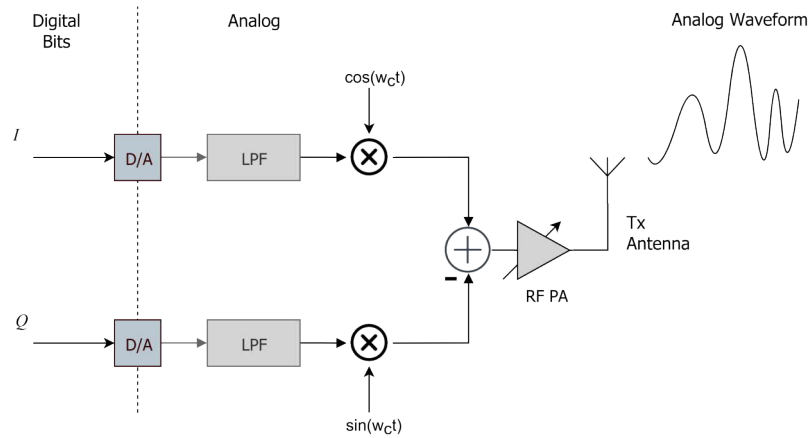


**Figure 3.2** General I/Q modulation block diagram. It states the main blocks for a complex modulation with in-phase and quadrature components.

The phasor representation of the signal in the Cartesian plane, in the real part and imaginary part (I and Q respectively), is represented with the Euler's formula ( $e^{j\omega t}$ ) in Eq. 3.3 [13]. The possibility to work with complex numbers facilitates the representation in a two-dimension plot, which is used to have a symbol alphabet. Such scheme representation is called constellation, where every symbol on it denotes a determined number of bits. There are different kinds, but quadrature amplitude modulation (QAM) and phase shift keying (PSK) are often used [73]. Meanwhile, the symbols are distributed on a uniformly spaced grid in QAM, in PSK are uniformly dispersed in a circle.

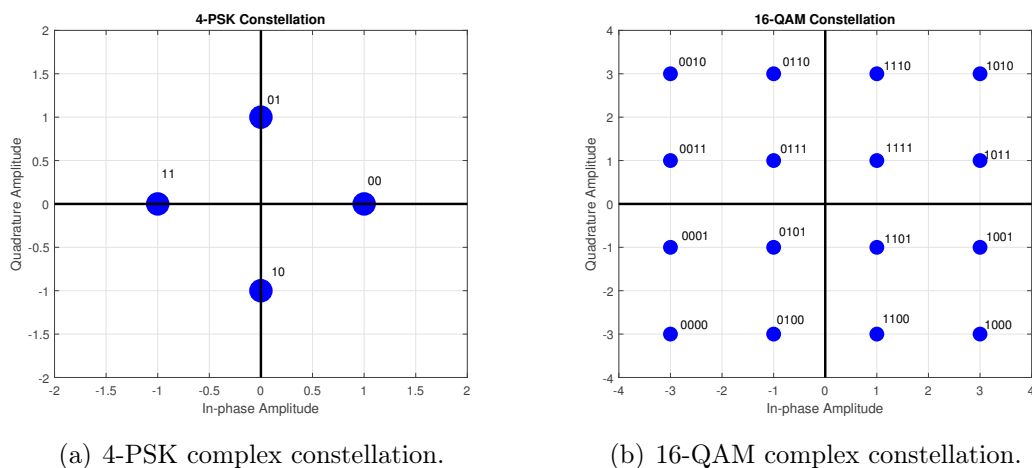


**Figure 3.3** Constellation examples for 4-PSK in (a) and 16-QAM in (b) with alphabet size of 2 and 4 respectively.

For instance, in Fig. 3.3, two complex constellation are presented. In 3.3(a), four symbols, each carrying two bits, are distributed evenly in a distance of one from the center of a circle (radius). On the other hand, in 3.3(b), each symbol carrying four bits, are spaced uniformly in a distance of one or three in quadrature or in-phase amplitude. The modulation schemes using constellation are several nowadays, for example, current Long-Term Evolution (LTE, standard for 4G mobile communications) uses 16-QAM and 64-QAM modulation scheme, meanwhile LTE-Advance Pro considers 256-QAM [77].

## 3.2 Multicarrier modulation And OFDM

The main objective of a multicarrier modulation is to use the total bandwidth available for the transmission, so that it is composed of numerous narrow bandwidths. Multicarrier techniques compared with single carrier methods brings many advantages, such as to improve the use of the total bandwidth, and to mitigate the attenuation due to multipath propagation, fading and interference [75].

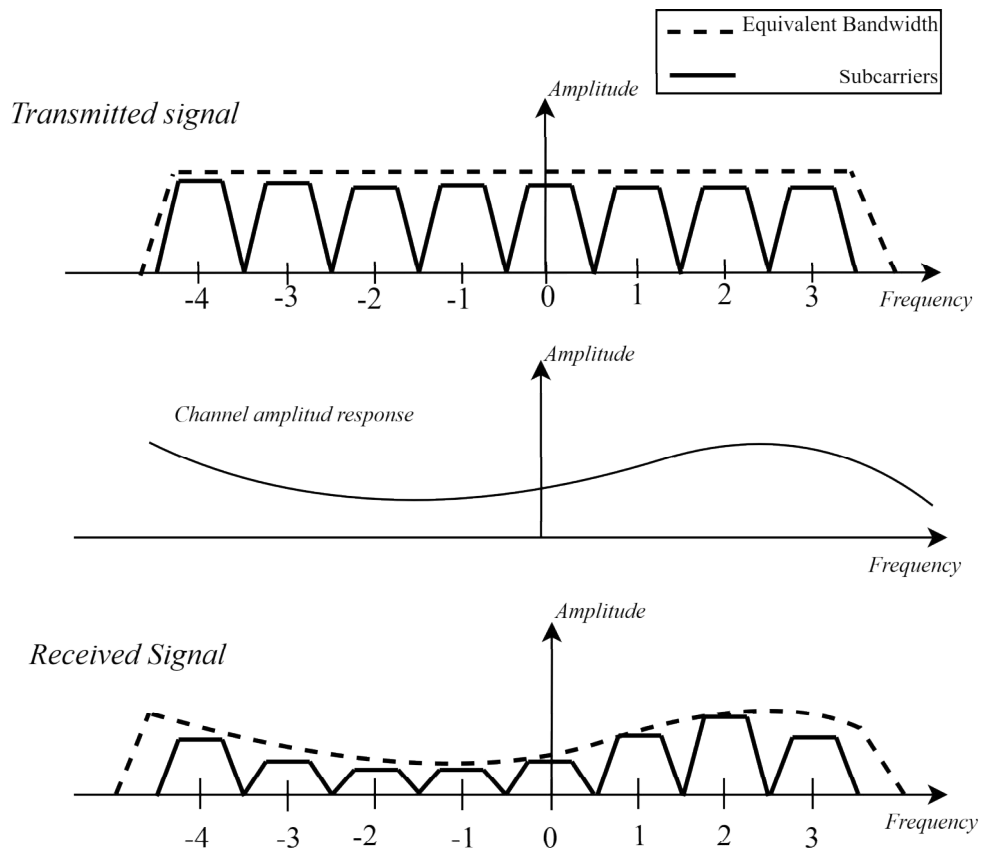


**Figure 3.4** Brief comparison between how the channel amplitude response affects over the transmitted signal with frequency-division multiplexing (FDM) technique. Where  $\Delta f$  is the frequency spacing, and  $[-4, -3\dots 2, 3]$  are the subcarrier index.

Figure 3.4 shows a general example on how a multicarrier modulation behaves against channel amplitude response. The narrowbands that integrate the whole bandwidth are attenuated after the transmission through the channel, and at the receiver side the obtained signal will have more attenuation in those subbands where the channel amplitude response is stronger. The figure represents a frequency-division multiplexing (FDM) technique to separate the subbands in the available bandwidth.

The multicarrier modulation, as in FDM (Fig. 3.4), has the disadvantage that in order to decrease inter-symbol-interference (ISI) every parallel subcarrier must be modulated with a spacing. Hence, limited subbandwidths mitigate the ISI effect, but the efficiency of the transmission decreases. One method to accomplish more subbandwidths within the available bandwidth, is to transmit orthogonal modulated signals. The orthogonal frequency division multiplexing (OFDM) allows to transmit numerous overlapped subcarriers, but uncorrelated to each other.

Figure 3.5 shows multiple sinc-shaped pulses overlapping each other in the frequency domain, which is a representation of eleven subcarriers individually shaped in an OFDM system. Every sinc-shaped pulse does not correlate to any other adjacent signal, due to the maximum amplitude (power) of every pulse coincides to one of the minimum values of other pulses [76].

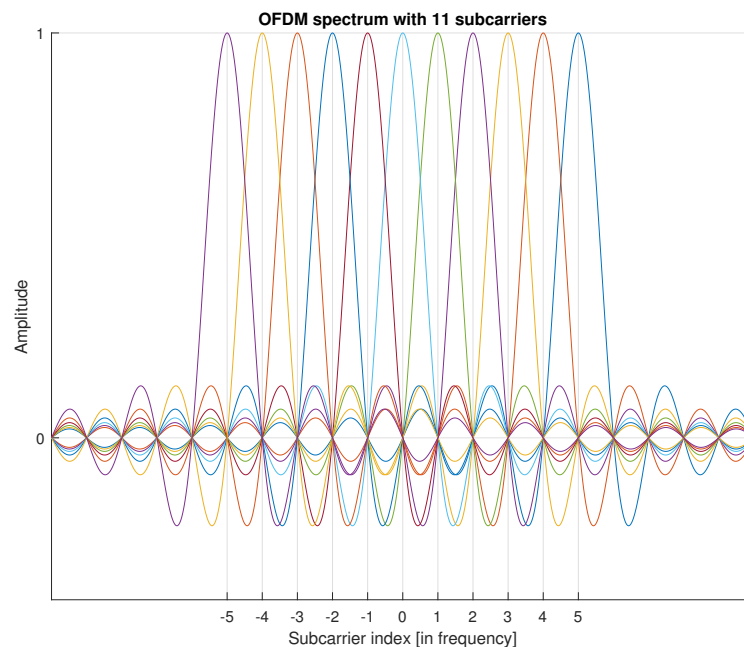


**Figure 3.5** Spectrum of eleven sinc-shaped subcarriers orthogonal to each adjacent pulse.

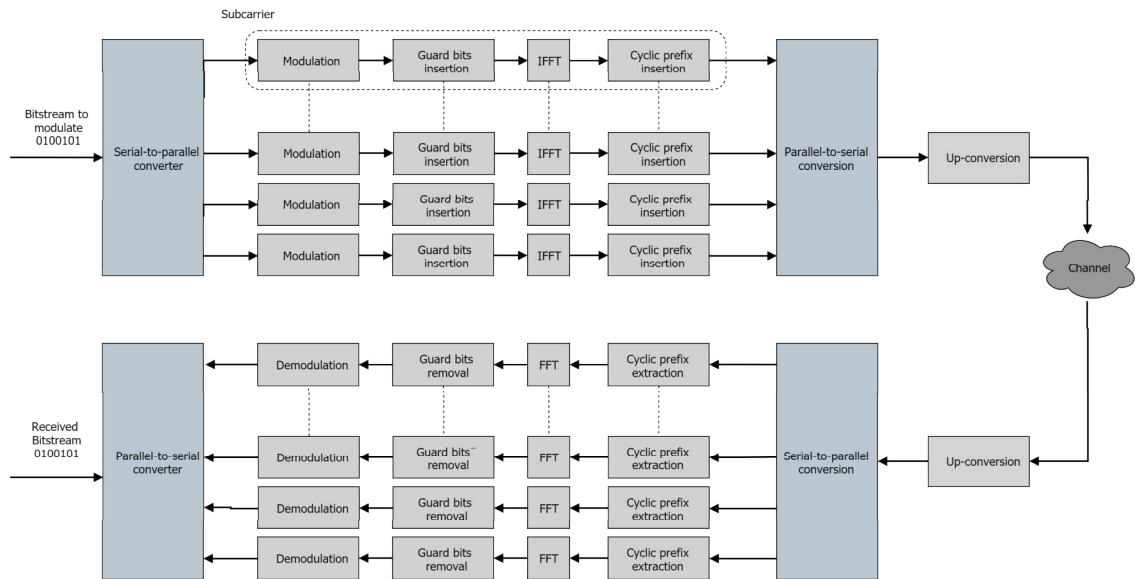


**Figure 3.6** General block diagram for a OFDM system.

Figure 3.6 illustrates a general block diagram for a OFDM system, which transmits a modulated signal carrying bits through a channel. Broadly speaking, the OFDM system is based on many subcarriers being sent in parallel, in the serial-to-parallel converter this is done by separating the bitstream into the individual subchannels. The process is inverse in the parallel-to-serial converter in the receiver side.

The guard bits insertion and the cyclic prefix insertion block are meant for forward error coding at the receiver side. For instance, the cyclic prefix is copying data from the initial part of the subcarrier and adding it to the end, increasing the duration of the transmitted symbol, which helps in the receiver side to fix errors, i.e. due to multipath [78].

The FFT and IFFT (fast Fourier transform and inverse fast Fourier transform) block in Fig. 3.6 modulates each subcarrier and transforms the signal from time into frequency domain (in case of FFT). In general, the FFT is a computational implementation of the discrete Fourier transform (DFT), which works at powers of two and optimizes the DFT. The signal at the transmitter is established in the frequency domain as discrete values (digital), defining each element of the signal according to the values in a discrete Fourier transform spectrum. Thus, the processing of a multicarrier signal with OFDM can be done with the implementation of a inverse DFT (IDFT), and in the receiver the inverse processing can be achieved with a DFT.

In a more mathematical approach, the output of a OFDM system can be expressed as the transmission of many complex waves (as in Eq. 3.1), and the modulation of

the output can be done with a IDFT procedure. Thus, the model of the OFDM output in a discrete-time can be implemented as an IFDT implementation, seen in Eq. 3.4. In the equation  $N$  is the total number of OFDM subcarriers,  $k$  is the frequency index of the symbol (subcarrier),  $n$  is the index on time,  $x(n)$  the signal in time, and  $X(k)$  the signal in frequency domain [75]. The IDFT from the time to the frequency domain generates symbols that are orthogonal.

$$x(n) = \frac{1}{N} \sum_{k=0}^{N-1} X[k] e^{j \frac{2\pi}{N} kn} \quad (3.4)$$

One big challenge in the OFDM, and multicarrier methods is the high peak-to-average power ratio (PAPR) that multiple waveforms generate. PAPR is the quotient between the square of the highest amplitude that the signal reaches by the square of the average value of the whole signal sent, as seen in Eq. 3.5. It is more probable to obtain high peaks when multiple sinusoidal waves are combined in comparison with single carrier waveforms. As a consequence, this leads into nonlinearities at the amplifiers in the transmitter and more distortion at the receiver side, being one of the main challenges of OFDM design [75].

$$PAPR = \frac{\max_{\{0 \leq t < T\}} |x(t)|^2}{E|x(t)|^2} \quad (3.5)$$

### 3.3 Power Amplification And Nonlinearity

In the transmission of a signal through a channel (e.g. the air) power amplifiers (PA) are considered, in order to ensure that the receiver will be able to obtain the transmitted data (or transferred power). There are different models for PAs, which are represented as mathematical expressions. These approximations are useful to characterize PA systems and to calculate approximated outputs for amplified signals by the PA.

Some generic memoryless power amplifier models are the soft envelop limiter (SEL), the Rapp AM-AM (instantaneous output envelope vs. input envelope), and the polynomial model. In a memoryless PA model, the values at certain time does not depend in the previous one. In the SEL model (Eq. 3.6), while the input ( $x(t)$ ) is less than the saturation threshold ( $x_{sat}$ ), the amplification is linear. However, if they are above the threshold, values clip and the PA transmits the saturation value instead. In case of the Rapp AM-AM model (Eq. 3.7), the output value depends in the threshold and a  $p$  variable that controls the shape of the upper-limits. The  $p$

parameter is selected according to the semiconductor of the PA.

$$f_A(x(t)) = \begin{cases} |x(t)|, & |x(t)| \leq x_{sat} \\ x_{sat}, & |x(t)| > x_{sat} \end{cases} \quad (3.6)$$

$$f_A(x(t)) = \frac{|x(t)|}{\left(1 + \left(\frac{|x(t)|}{x_{sat}}\right)^{2p}\right)^{\frac{1}{2p}}} \quad (3.7)$$

The SEL (red line) and The Rapp AM-AM (purple line) models are presented in Fig. 3.7, where is seen the relation between input and output and the threshold level at certain output value. It is seen also in the plot both methods compared with the linear behavior (in blue). In case of the Rapp AM-AM model, it has a  $p$  value equals to 2.5. For instance, in Fig. 3.7, the input voltage must be under 1 to avoid clipping in the output. Between 1 and -1 the PA has a linear behavior, after those limits the output gets clipped and starts to give the same value even though the input increases. When values in a PA are clipped means that the output are not as desired and expected when working in the linear region, and non linearities appear [13].

In systems with high PAPR, as in OFDM, is more probable to pass the threshold. Thus, high PAPR produces more nonlinearity in the final transmitter signal.

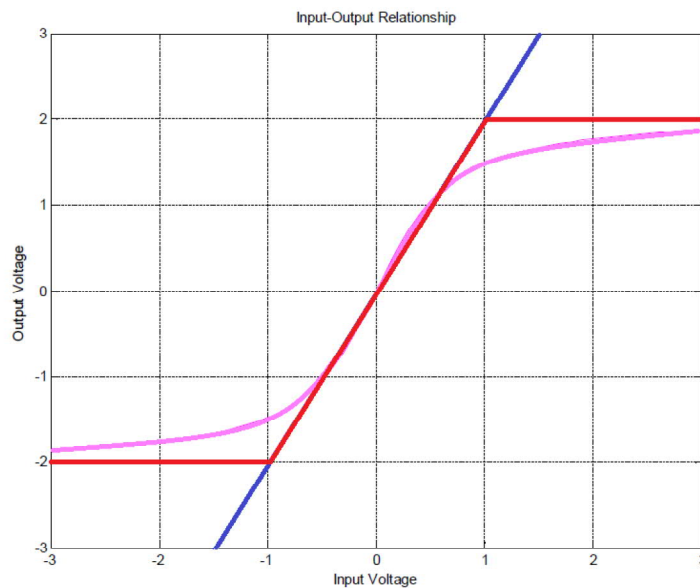


**Figure 3.7** PA model diagram for SEL (in red) and for Rapp AM-AM with  $p = 2.5$  (in purple).

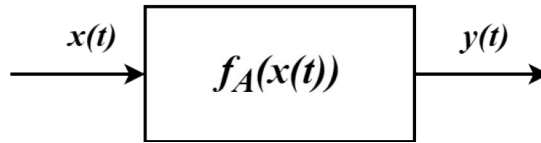


**Figure 3.8** Simple nonlinear system considered in equation 3.9. Where input  $x(t) = \cos(wt)$  is replaced in the system representative equation and the result is obtained in the output  $y(t)$ .

In a polynomial model (Eq. 3.8) it is possible to model the output of a PA, by knowing the equation that represents the output of a nonlinear system. The system is described as a polynomial function, as in the example in Eq. 3.9.

$$f_A(x(t)) = \sum_{n=0}^N A_n [x(t)]^n \quad (3.8)$$

For example, in case the system in Fig. 3.8 is modeled as a third order polynomial, it is possible to observe how new frequencies are generated due to the nonlinear behaviour of the system, these new elements in the spectra of the signal are called harmonics.

$$\begin{aligned} y(t) &= \cos wt + \cos^2 wt + \cos^3 wt, \\ y(t) &= \cos wt + \frac{1}{2}(1 + \cos 2wt) + \frac{1}{4}(\cos 3wt + 3 \cos wt), \\ y(t) &= \frac{1}{2} + \left(1 + 3 \cdot \frac{1}{4}\right) \cos wt + \frac{1}{2} \cos 2wt + \frac{1}{4} \cos 3wt, \\ y(t) &= \frac{1}{2} + \frac{7}{4} \cos wt + \frac{1}{2} \cos 2wt + \frac{1}{4} \cos 3wt, \end{aligned} \quad (3.9)$$

In Eq. 3.9 is considered the equation that describes the system function ( $F_A(x(t))$ ) as  $x(t) + x^2(t) + x^3(t)$ . The system function is described as a polynomial equation of third order, so the output signal is a sum of the same element (input signal) to the power of one, two and three. Apart of the frequency of the input signal ( $w$ ), the output  $y(t)$  has harmonic frequencies generated from the cosines to the power of two and three. The 2<sup>nd</sup> and 3<sup>rd</sup> order harmonics are possible to see in the final line of Eq. 3.9, these new frequency will appear at the spectra of the signal as new peaks with less amplitude than the original but still considerable to distort the output signal.

## 4. TESTBED STRUCTURE

This chapter explains the implementation made to achieve the primary objective of the present thesis project, i.e., to create a research testbed for RF power transfer using a USRP SDR. The testbed is integrated with a SDR and a USB meter at the transmitter side, and with a RF-to-DC converter, an ADC and a microcontroller in the receiver side, as shown in Fig. 1.1. Additionally, the central component is a computer running a custom software, which is in charge of the transmission with the SDR and to synchronize the data acquired from the receiver side.

A more detailed description of the selected devices and employed for the testbed implementation are presented in four sections as follows. Section 4.1 describes the devices used to implement the transmission of any given signal and to gather information related to the power that the SDR consumes from the PC. In Section 4.2, the following numerous devices are thoroughly described: the RF-to-DC converter, the ADC and the microcontroller reading the voltage of the harvested DC as well as the procedure for communicating these values to the computer. The final structures implemented for the transmitter and receiver side are in sections 4.3 and 4.4, respectively. In Section 4.5, the final prototype is presented, in which both implemented sides with all previous devices are connected. Finally, in Section 4.6, the programs made to achieve the main objectives of the custom software, such as the transmission of any given signal saved in a file, the acquirement of the data from the microcontroller and others program functionalities are explained.

### 4.1 Transmitter Side

The transmitter side has mainly two blocks: the supplied power, and the SDR block (Fig. 1.1). This side performs the broadcasting and also measures the power that the SDR uses at the transmission stage.

### 4.1.1 Software Defined Radio (SDR), USRP

Software defined radios are devices that wirelessly transmit (or receive) RF signals, and all the physical layer functions are software defined. The SDRs devices are built with some (or all) RF operating functions over programmable processing technologies, using components such as field-programmable gate array (FPGA), digital signal processors (DSP), general purpose processor (GPP), and programmable system on chip (SoC) [79].

The selected SDR device to broadcast any given waveform in a file or to transmit adaptively is the Ettus Research (a National Instrument brand) USRP-2900. It can be used as a tunable transceiver working from 70 MHz to 6 GHz frequency range. Additionally, the USRP-2900 uses USB 3.0 bus-powered connection, allowing high speed data communication and power source. The selected SDR works exclusively as a transmitter in the testbed system is restricted to the transmission of a signal. The most important operational characteristics of the USRP-2900 are summarized in Table 4.1 [80].

Due to the FPGA in the USRP, it is achievable to upload a firmware in it and set different parameters for the transmission ("Transmission Control" block in Fig. 4.1). For instance, USRP-2900 can be set between any frequency in the range from 70 MHz to 6 GHz.

**Table 4.1** USRP 2900, Transmitter characteristics.

Parameter	Value
Frequency range	70 MHz to 6 GHz
Frequency step	<1 kHz
Maximum output power ( $P_{out}$ )	20 dBm
Gain range	89.75 dB
Gain step	0.25 dB
Frequency accuracy	0.25 dB
Maximum instantaneous real-time bandwidth	56 MHz
Maximum I/Q rate	
Streaming	15 MS/s
Burst	61.44 MS/s
Digital-to-Analog converter (DAC)	12 bits

The block diagram for the USRP 2900 working as a transmitter is illustrated in Fig. 4.1, where the computer and the USRP are connected through a USB 3.0 bus. It is also seen the two branches representing the I/Q modulation for the output signal, with their digital up converter (DUC), digital-to-analog converter (DAC) and lowpass filter. Thus, digital data are up-converted, then transformed into an analog signal (DAC) according to the sample rate of the signal, and finally passed

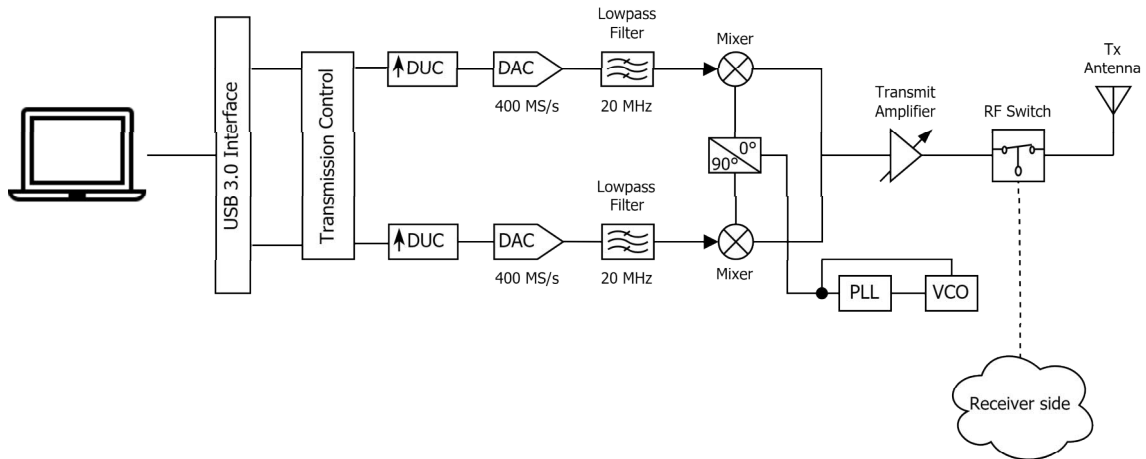


**Figure 4.1** Block diagram of the USRP-2900, due to its FPGA it is possible to set the transmission with different parameters. The receiver side is ignored because the testbed SDR is exclusively used as a transmitter.

through a low pass filter. In order to I/Q modulate the signal, the dis-phase block is allocated for both branches with 0 and 90 degree dis-phase for the I and Q branch respectively. As explained in Chapter 3, the I and Q components are combined before the transmission, but they are 90 degree dis-phased, the PLL (Phase-locked loop) and VCO (voltage controlled oscillator) are in charge of this procedure. Finally, a gain amplifier is in charge to set the gain level defined in the parameters at the computer (i.e. in Fig. 6.3(a)).

### 4.1.2 Power Meter

The supplied power by the computer to the USRP is measured with a USB power meter manufactured by YZXstudio, model ZY1273. The device can measure the voltage and the current that the computer supplies for transmitting in the USRP. The values from the USB power meter can be read through a parallel connection from the USB power meter with a USB to TTL (transistor-transistor logic) cable connection.

The USB power meter specifications are listed in Table 4.2 [81]. The most relevant characteristics are the resolution in the voltage and current measurements, because the testbed calculates the power with these values.

The power meter shows several measured values in its display; voltage, current, watts, ohms, watts per hour, amperes per hour, and even the temperature. Moreover, the device has different screen mode displaying aforementioned values, and including a chart mode where voltage and current are plotted in the display.

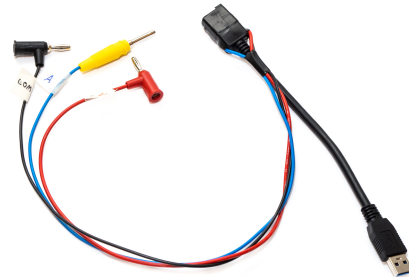
**Table 4.2** USB power meter ZY1273 specifications.

Parameter	Value
Input voltage	3.5V-24V
Input current	$\pm 5A$
Voltage resolution	0.1mV
Current resolution	0.0001A
Cumulative capacity	0-99999Wh
Capacity resolution	0.0001Wh
Accuracy	
Voltage	0.1%+2d
Current	0.2%+2d
Wh capacity	0.5%
Display	1.3" 128x104 pixel Colour TFT
Update rate	Every 0.36s
Idle current consumption	8mA / 6mA (with display dimmed/off)
Current shunt resistance	10m $\Omega$
Overall circuit resistive loss	42m $\Omega$
USB type	USB 3

More specifically, the TTL to USB converter cable employed is the TTL-232RG-VREG3V3-WE manufactured by FTDI Chip. This cable provides the values taken by the USB power meter to the computer as a serial communications. The main technical specifications are the USB to UART with +3.3V TTL level UART signal and the maximum current output of 50mA on VCC [82]. The implemented USB power meter with the TTL to USB converter cable is shown in Fig. 4.2(a).



(a) ZY1273 USB power meter with TTL to USB cable



(b) USB cable with parallel connection for multimeter measurements

**Figure 4.2** In (a) the ZY1273 USB power meter hardware is connected with TTL to USB cable. In (b) the USB cable modified with a parallel connection to cables with banana connectors for measurements with external multimeter is shown.

Additionally, there is another method to obtain measurements of the supplied power from the computer. It was designed a USB cable with a parallel connection to banana jacks, making possible the measurement of the supplied power with an external multimeter, as shown in Fig. 4.2(b).

The main difference between the two methods for measuring the supplied power is the procedure in which the information is obtained. For example, operational assessments in Chapter 6 were carried out with the USB cable with parallel connection to the multimeter. The values are taken by observing the multimeter and writing down the values in a table, meanwhile with the USB power meter those values can be ordered, i.e. in a CSV file. However, the writing in a CSV file the values obtained from the USB power meter has not been implemented, and it can be considered for future work.

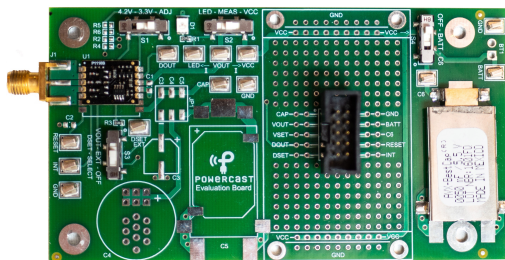
## 4.2 Receiver Side

The receiver side is composed of three main blocks, as seen in Fig. 1.1, the RF-to-DC converter, the ADC converter, and the microcontroller. The elements in the receiver structure work jointly to obtain the transmitted signal, convert RF-to-DC, read the DC generated voltage, and deliver the information to the computer.

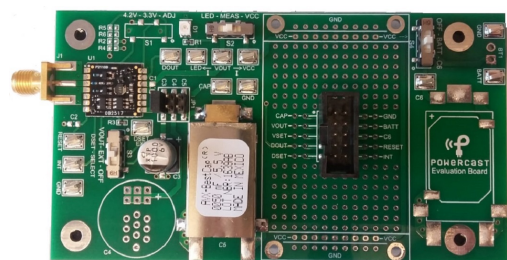
### 4.2.1 RF-to-DC Converter, Power harvester <sup>®</sup>

The employed RF-to-DC converters in the testbed are P2110 and P1110 EVB models manufactured by PowerCast. These harvesters are receiver devices for conversion of the RF signal transmitted from the SDR. Besides, both EVBs have high conversion efficiency at their optimal operation frequency range (902-928 MHz). Furthermore, these boards are selected due to their broad use in WPT research [65–72, 83].

Figure 4.3 shows that the EVBs are built similar and almost with the same components. However, P1110 shown in Fig. 4.3(a) does not present a boost converter and storage of the DC harvested through a capacitor, like P2110 shown in Fig. 4.3(b).



(a) P1110 EVB Hardware



(b) P2110 EVB Hardware

**Figure 4.3** The P1110 in (a) and the P2110 in (b) are the RF-to-DC converters used in the implementation at the receiver side of the testbed.

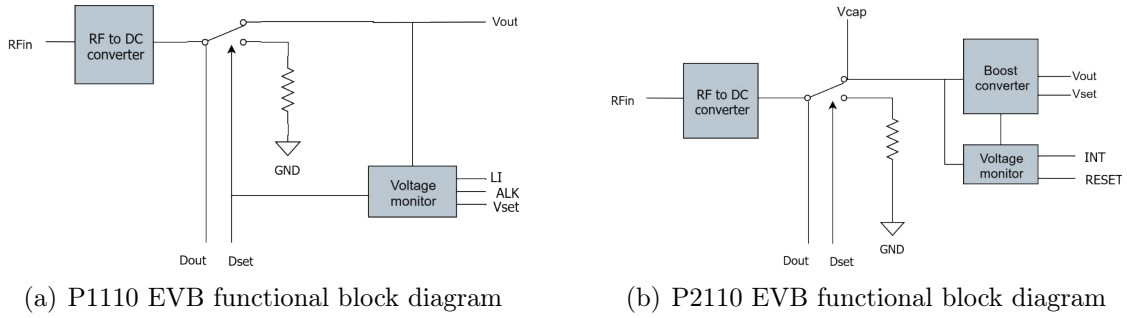


**Figure 4.4** RF-to-DC converters used in the implementation at the receiver side of the testbed.

The functional block diagram for both EVBs are shown in Fig. 4.4, it is explained that both boards have a resistor component in which the generated DC in the chip-set goes through if a switch is driven high. The boost converter and the  $V_{cap}$  (capacitor storage) in P2110 are shown in Fig. 4.4(b), meanwhile these components are not in P1110 shown in Fig. 4.4(a). The EVBs have other outputs that are not used in the implementation of the testbed, such as the digital output which indicates voltage is present in  $V_{out}$  (INT) and the digital input set to disable the  $V_{out}$  (SET) in P2110 (Fig. 4.4(b)) [84]. Similarly, in P1110 EVB the output to recharging with Li-ion/LiPo pin (LI), the alkaline recharging pin (ALK), and the maximum output voltage adjustment ( $V_{set}$ ) are not employed in P1110 (Fig. 4.4(a)) [85].

**Table 4.3** Switch selection for RSSI mode at the EVBs.

Switch	Position
S1	ADJ (Only in P1110)
S2	MEAS
S3	EXT

$$P_{[mW]} = \frac{V_{D_{out}}^2}{R_{EVB}} \quad (4.1)$$

The EVBs are configured to work in the received signal strength indicator (RSSI) mode, which is selected as shown in Table 4.3. The switches position shown in Table 4.3, switch S1 must be selected as ADJ to not use the resistor for optimized the harvested voltage, switch S2 must be in the position MEAS for measuring the resistor where the harvested voltage can be measured, and S3 must be selected as EXT for enabling external  $D_{set}$  to drive high the switch explained in Fig. 4.4. The RSSI mode gives the voltage that the RF-to-DC harvests, and this voltage is employed to calculate the power related to the transmitted waveform.

**Table 4.4** Identifier for every EVB used in the testbed.

Model + Number	Resistor value $R_{EVB}(\Omega)$
P1110B 001	49.9
P1110B 002	49.8
P2110B 003	287.6
P2110B 004	286.1

The power is calculated with the square of the voltage at the  $D_{out}$  multiplied with the resistor in which the voltage generated is measured, as seen in Eq. 4.1. The specific resistor values for every EVB that the testbed uses and the identifiers proposed for them are shown in Table 4.4.

### 4.2.2 Analog-to-Digital converter, ADS1115

The ADS1115 manufactured by Texas Instruments is selected as the ADC to read the analog voltage generated at the harvester and communicate this data as bits with the microcontroller. In Figure 4.5, the hardware of the ADC is shown.

The device main characteristics are the high resolution ADC 16 bits, the programmable gain amplifier (PGA) included for different ranges resolution, two functionalities mode (one-shot and continuous), and the small size package. Moreover, the ADS1115 specifications are summarized in Table 4.5 [86].

A special caution for the ADC device set up has to be taken into account, because it works in a range of -0.3 V to +5.5 V and this value has to be considered in the input voltage to GND, as seen in Table 4.5. For example, if the DC generated by the harvester fluctuates out of the -0.3V to VDD+0.3V range, it can be detrimental and even resulting in a total destruction of the chip-set in the board, this happened to one port in one ADC during the test stage.



**Figure 4.5** The ADS1115 is a high-resolution ADC converter used in the testbed for purposes to read the generated voltage at the harvester, and to communicate this data (as bits) with the microcontroller.

The device has two main operative modes, single-shot and continuous conversion. The single-shot mode is intended for conversions with power saving, periodic ADC conversions or long idle times between readings. On the other hand, the continuous conversion mode, the device starts to convert immediately after the previous conversion is made in the input of the ADC, the implemented testbed employs the ADC as continuous mode.

In the testbed implementation the ADS1115 is set in continuous mode to communicate the read data with the microcontroller. The communication between the ADC and the microcontroller is a I<sup>2</sup>C bus connection, therefore, in both devices the data line (SDA) and clock line (SCL) pins are used. Furthermore, because the device is connected particularly with one RF-to-DC receiver, the ADC works primarily for one connection. However, the ADS1115 has four input pins that can be used for parallel measurements, four devices connected with one ADC [86].

*Table 4.5 ADS1115 maximum values.*

Parameter	Maximum value
VDD to GND	-0.3V to +5.5V
Analog input current	100mA, momentary
Analog input current	10mA, continuous
Analog input voltage to GND	-0.3V to VDD +0.3V
Maximum sample rate (SPS)	860

*Table 4.6 ADS1115 PGA scale.*

PGA setting	Full Scale range (V)
2/3	±6.144
1	±4.096
2	±2.048
4	±1.024
8	±0.512
16	±0.256

### 4.2.3 Microcontroller, Arduino Nano

The device in charge of the proper synchronization and control the communication of data in the receiver side is the microcontroller. The microcontroller manages the voltage measured at the ADC (Master-slave connection through the I<sup>2</sup>C bus), besides, it communicates these values to the main program at the computer.

The device selected to fulfill the requirements is Arduino Nano, manufactured by the Arduino Company. The open-source hardware is a small device (Fig. 4.6) with a ATmega328 microcontroller chipset, which is the same in the broadly used Arduino UNO. Furthermore, the technical specifications of the device can be summarized in Table 4.7 [87].

Arduino Nano can be powered with the computer through its Mini-B USB connection, and also with an external source (6-20V). Nevertheless, an external power source is not needed because the microcontroller is all the time connected with the

**Table 4.7** *Arduino Nano specifications.*

Parameter	Value
Microcontroller	ATmega328
Operating voltage	5V
Flash memory	32 kB
SRAM	2kB
Clock speed	16 MHz
Analog IN pins	8
EEPROM	1kB
DC current per I/O pins	40 mA
Input voltage	7-12V
Digital I/O pins	22 (6 of them PWM)
PWM output	6
Power consumption	19mA

computer when the testbed is running. Therefore, communication with the computer is done with USB 2.0 protocol connection. Once the device is powered, it is feasible to program the pins to deliver voltage or to read incoming voltages.

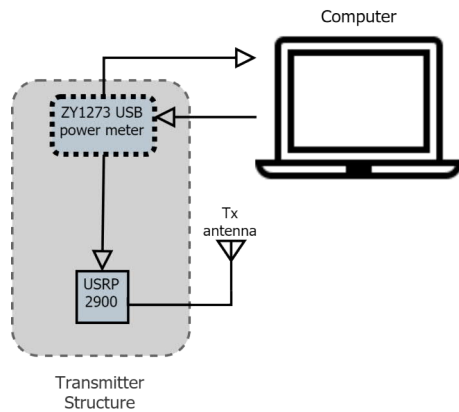
The Arduino software (IDE) is the interface used to upload the program in the memory of the device, as well to upload parameters (e.g., values from Table 4.4) in the electronically erasable programmable read-only memory (EEPROM) of Arduino nano. Programs related to the testbed will be explained in more detailed in Section 4.6.



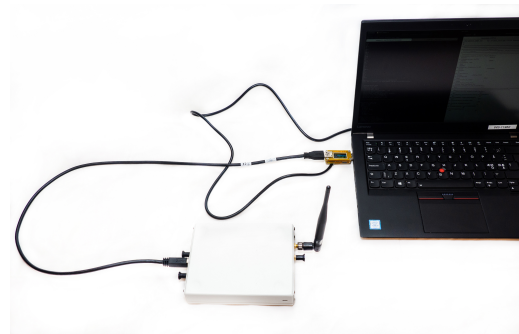
**Figure 4.6** *Arduino Nano used in the testbed implementation. It has similar performance as the broadly used Arduino UNO, with a ATmega328 microcontroller. The device is selected due to its small size and good performance in the acquisition and communication with the computer.*

### 4.3 Final Transmitter Structure

The final transmitter structure diagram can be seen in Fig. 4.7(a), where the USRP 2900 and the ZY1273 USB power meter are connected with the USB port at the computer. The power meter works as a bridge between the USRP and the computer, it measures the instantaneous voltage and current and transmits these values to other USB port at the computer thanks to the USB TTL cable.



(a) Final transmitter structure diagram



(b) Final transmitter structure implementation

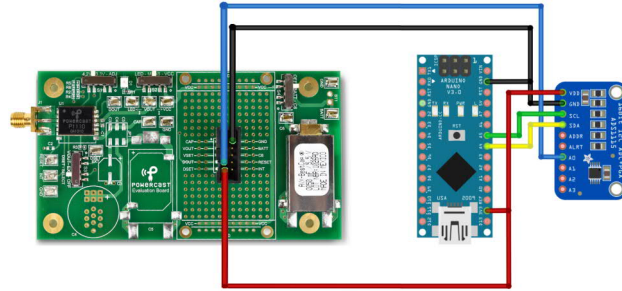
**Figure 4.7** Final structure diagram (a) versus the final implementation (b) for the transmitter side.

The final structure for the transmitter implemented hardware is shown in Fig.4.7(b). Because the USB 3.0 connection that the USRP 2900 and the ZY1273 USB power meter support, the transmission can operate without interruption or disconnection in the operational performance.

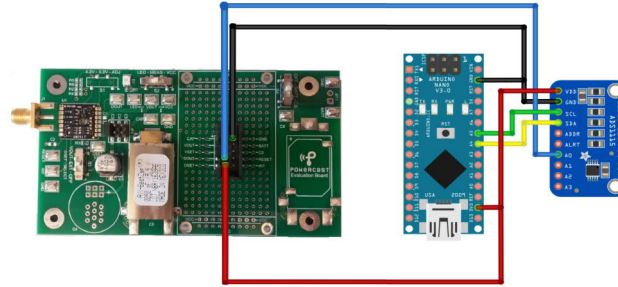
The final configuration for the transmitter can include an antenna Siretta Delta 6A which is attached to the USRP, as seen in Fig.4.7(b). The selected antenna is designed to transmit at quad bands GSM frequencies, such as 868 MHz, 915 MHz, and 2100 MHz.

### 4.4 Final Receiver Structure

Figure 4.8 shows the two wire schematics designed for the data acquisition from the harvester and following data delivery to the computer through the microcontroller. An ADS1115 ADC converts the voltage measured at the  $D_{out}$  pin in the harvester. At the same time, Arduino nano controls the ADC through an I<sup>2</sup>C, reads the analog data converted into bits, and sends this information to the computer.



(a) Wire schematics for the receiver structure with P1110 EVB

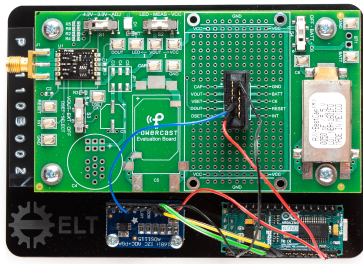


(b) Wire schematics for the receiver structure with P2110 EVB

**Figure 4.8** The wire schematics designed for purposes to measure and communicate the RF-to-DC conversion done at the harvester. The implementation of the receiver side with P1110 in (a) and in (b) with P2110.

Figure 4.8 shows that the components are the same with exception of the RF-to-DC converter, P1110 in 4.8(a) and P2110 in 4.8(b). It is also shown that the  $D_{set}$  pin at the harvester and the VDD pin at the ADC are connected in parallel with the output 3.3V pin in the Arduino. Similarly, the GND (ground) pins at the EVB and the ADS1115 devices are connected with Arduino nano GND pin.

In the implementation of the testbed a total of four receiver were created, two employing P1110 EVB (Fig. 4.8(a)) and two with P2110 EVB (Fig.4.8(b)). For instance, in Fig. 4.9 one of the four final hardware structure for the receiver side is illustrated. The final receiver hardware has all devices fixed in a laser-cut fiber glass structure, and the connection is done through soldered cables in proper connectors for every device. In addition, to use the receiver for acquisition of a waveform an antenna can be added to the harvester. For example, in Fig. 4.9(b), a PCB dipole included with the EVB package with maximum efficiency at 915 MHz is utilized. Besides, the switch configuration must be as in Fig. 4.9(a) (according to Table 4.3), to employ the RSSI mode of the EVBs.



(a) Final receiver structure with EVB in RSSI mode.



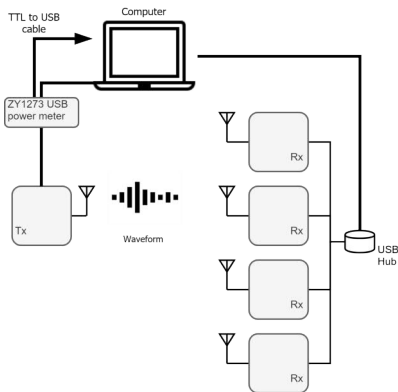
(b) Final receiver structure with attached antenna

**Figure 4.9** Final receiver hardware in a lase-cut fiber glass structure, where all devices are jointly connected. The harvester can be connected with a dipole antenna as show in (b). In Fig. (a) the switch configuration stated in Table 4.3 is shown for selection of the RSSI mode.

## 4.5 Final Testbed Implementation

Figure 4.10 illustrates and shows the configuration of the final result for the testbed implementation. The final diagram of the testbed created can be seen in Fig. 4.10(a), while the final setup achieved is shown in Fig. 4.10(b).

The practical implementation is shown in Fig. 4.10(b), where all devices selected in the design of the testbed are connected to the computer with the main program. Additionally, it is shown than the receivers can be aligned and located as far as possible due to the long cables attached to them.



(a) Final diagram setup



(b) Final testbed setup

**Figure 4.10** In (a) is the diagram of the achieved testbed with all receiver blocks jointly connected. In addition, the testbed in practice is displayed with all the devices connected in (b).

**Table 4.8** Notebook computer specifications used in testbed.

Software specifications	
Operating System	Linux
Release	Ubuntu 18.04 (bionic)
GNOME	3.28.2
Kernel	4.15.0-34-generic
GCC version	7(x86_64-linux-gnu)
Cmake version	3.10.2
Hardware specifications	
Vendor	Intel
Cores in the CPU	4
CPU Model name	Intel®core™i5-7200U CPU @ 2.50 GHz
Computer model	Lenovo Thinkpad T470s

## 4.6 TestBed Software

The testbed software consists in three primary programs, the master program at the computer, a slave program at the Arduino flash memory, and the code to write in the long-term Arduino memory (EEPROM) in a configuration stage.

All the programs are built in a notebook computer with a Linux operating system (OS). The main reason of the selection of the aforementioned OS is the capability to compile C++ codes at the terminal by using GCC (GNU compiler collection) commands. Besides, the chance to manage multitask processes and access the serial ports connected at the same time. In the selected OS the installation of libraries and needed dependencies to employ the USRP is straightforward, as explained in a following subsection. More details of the hardware and software of the PC used in the test are given in Table 4.8.

### 4.6.1 Main Program

The main program in charge controlling and synchronizing all processes of the testbed is a code written in C++ programming language. This code is compiled and executed at the computer, then a default image pre-installed at the FPGA in the USRP runs the transmission with the instructions in the C++ program.

### UHD Dependencies And Repository Installation

To control the USRP with C++ language codes, the installation of the USRP hardware driver (UHD) software is needed. The UHD is a free and open-source driver

created for USRP by Ettus Research and it is supported in Linux OS. For example, there are several known toolkit using UHD, such as GNU Radio, NI LabView, Mathworks Simulink, and Software Radio System LTE to name a few [88].

As explained in [89], to build dependencies of the UHD in a Linux OS, there are some requirements for the system. For instance, C++ GCC has to be newer than version 4.8 and the Cmake newer than version 2.8. The next step after updating the basic requirements is to install the dependencies, according to the Linux distributor (e.g. Ubuntu). When dependencies are installed, it is feasible to obtain the UHD source from a git repository. The instructions for the installation of dependencies and repository on Ubuntu from the source code are summarized with the command codes in Table 4.9.

*Table 4.9 Installation of the UHD dependencies and repository.*

<b>1</b>	<b>Obtaining repository from Github.</b>
	<code>git clone git://github.com/EttusResearch/uhd.git</code>
<b>2</b>	<b>Generating Make files with Cmake</b>
<b>2.a</b>	<code>cd &lt;uhd-path-installation&gt;/host</code>
<b>2.b</b>	<code>mkdir build</code>
<b>2.c</b>	<code>cd build</code>
<b>2.d</b>	<code>../</code>
<b>3</b>	<b>Building and installing</b>
<b>3.1</b>	<code>* in &lt;uhd-path-installation&gt;/host/build)</code> <code>make</code>

Thus, according to Table 4.9, after the UHD repository is copied at the computer directory in Step 1, the generation of the Make files with Cmake is done in step 2. The step 3, building and installing of the libraries dependencies, is the following and final step.

To assess the correct setting-up of the UHD all the executables of the examples in the folder `<uhd-path-installation>/host/build/examples` must be created. If everything is installed properly, all the examples in the folder will run when executed along the USRP connected to the computer.

One method to create a separated C++ code and compile it with CMake procedure is with the example file in the folder `<uhd-path-installation>/host/examples/init_usrp/init_usrp.cpp`. Contrarily to the previous examples built, the "initialization" example code can be compiled apart from the UHD tree source, by following the steps 2 and 3 in Table 4.9. Furthermore, the `CMakeList.txt` in the `<uhd-path-installation>/host/build/examples/init_usrp` folder can be

modified to change the name of the executable. Besides, in case of moving the folder to another path in the computer, the libraries must be selected static in the CMakeList.txt file before the installing with steps 2 and 3. To do so, the line option(UHD\_USE\_STATIC\_LIBS OFF) must be changed to option(UHD\_USE\_STATIC\_LIBS ON). For instance, the main program developed and implemented in the testbed was made following the previous steps. In addition, the testbed main C++ code is based in the file tx\_samples\_from\_file.cpp from the example folder (<uhd-path-installation>/ host/ examples).

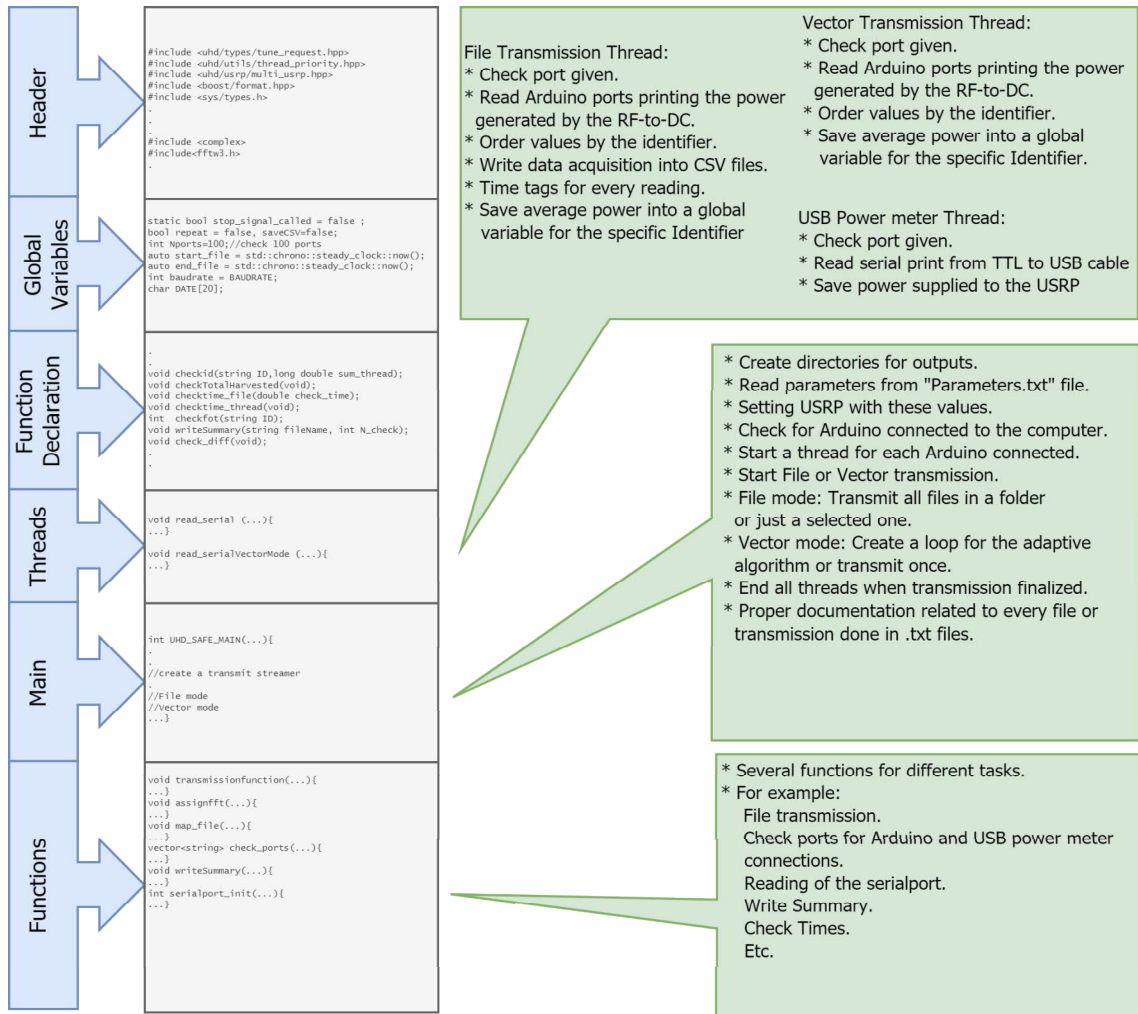


**Figure 4.11** The diagram of the main program design. It is written in a C++ structure and has three main sections: the threads, the main, and the functions. There are some example lines taken from the code used in the testbed implementation.

## C++ Program Structure

The structure of the testbed main program written in C++ language can be summarized in Fig. 4.11. There are three main sections in the program: the threads for different parallel processes, the main part controlling the program and calling the threads and functions, and the functions which are called to do different tasks.

Figure 4.11 illustrates how the program is written in a C++ manner. For instance, it starts with the declaration of the libraries in the header, global variables, functions, and the threads used for multitasking. In the code, after the main section, the functions to carry out different tasks are located.

```

1  for (int i = 0; i < sizeVec; i++) { // spawn n threads:
    futureObj[i]=exitSignal[i].get_future();
3  threads[i] =
    thread(&read_serial, ports[i], nameOfFile, move(futureObj[i]));
5  }
    start_file = std::chrono::steady_clock::now();
7

9  //Start transmission
    int LT= 0;
11 if(N_times==0)
    {cout<<"TRANSMISSION TIMES = 0, CHECK PARAMETERS!!"<<endl;
13  return EXIT_SUCCESS;}

15 do{
    transmissionfunction(tx_stream, buffD, spb);
17  LT+=1;
    } while(LT!=N_times and not stop_signal_called);
19 end_file = chrono::steady_clock::now();
    chrono::duration<double> diff_file = end_file-start_file;
21

    //end n threads
23 for(int i=0;i<sizeVec;i++){
    exitSignal[i].set_value();
25 threads[i].join(); }

```

**Program 4.1** Extract of the C++ code where the transmission in file mode is executed. It is seen the threads are spawned before the transmission of the file. The threads created depend in the number of Arduinos connected.

The threads are parallel processes working at the same time with the main one, which is the transmission of a waveform. There are three developed functions to implement multitasking while transmission is running, two of them depend in the selected mode to broadcast. As seen in Fig. 4.11, the threads File Transmission Thread and vector transmission thread are basically the same, they read the Arduino serial port and save the data acquired according to the identifier of the harvester. However, they

differ in the CSV file generation to save the data record received with time tags.

Vector transmission mode in the testbed does not have the option to save a CSV file, it uses the vector transmission thread to fulfill faster readings and returns just the average power obtained, this mode is implemented for adaptive transmission. Finally, the third thread is meant for readings from the USB power meter and saving an average value of the supplied power to the USRP in a global variable.

In case of the final implementation of the testbed there are four receivers, therefore, there are four threads created (vector transmission or file transmission) plus one thread to read the USB power meter serial connection. The synchronization of the readings from the microcontroller is based in the time that the ADC takes to start to read appropriate values and the following acquirement in the computer. Approximately one second is taken into account on threads to start to read values, for example, this was measured in assessments shown in Fig. 4.12.

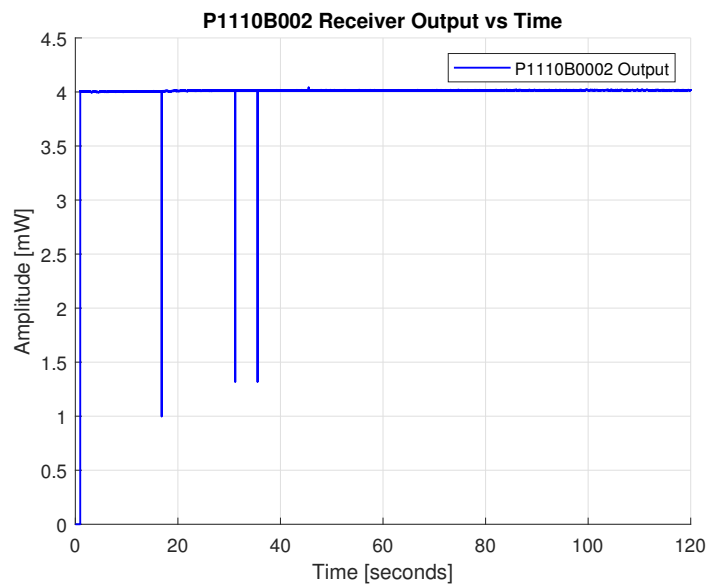


**Figure 4.12** Approximately one second is the time for the receiver side to start reading appropriate values according to the transmission side. These measurements were done with a complex tone signal at 200 kHz and in a wired connection.

The threads for reading the Arduinos ports are executed when the transmission starts, almost in parallel. Similarly, when the broadcast ends, all threads created are terminated and the information gathered (obtained average power of the signal) is saved in global variables. The procedure also depends in the total number of Arduinos connected to the computer. For example, a small part of the code is shown in Program 4.1, where the threads are started in a vector of the same size as Arduinos connected to the computer.

The settings of the USRP parameters are obtained from a file called `Parameters_USRP.txt` in the same folder where the code is. The main section in the program takes all the values and sets the transmission values. Besides, the mode selection (File or Vector transmission), to obtain the results in CSV files, to transmit N times, and control the adaptive transmission are possible to configure from the `Parameters_USRP.txt` file. More explanation and an example are found in Chapter 5. The purpose of having an external file to set parameters is to avoid unnecessary recompiling of the software.

The last part of the code is integrated with several functions for different tasks. The most important functions are the transmission and the initialization of serial ports which are always executed. The first one takes all the setting values for the USRP and sets the transmission (as in Program 4.1), the second function checks the serial ports connected and to set the reading.

### 4.6.2 Subprogram In Microcontroller

The Arduinos in the receiver structures are uploaded with a program in their flash memory. Besides, the EEPROMs of the microcontrollers are also used to save a structure with the identifier of the harvester and the value of the resistor where the voltage is measured.

#### Program To Write In The EEPROM

The Program 4.2 shows the designed code to write parameters in the EEPROM. The code is taken from the program written in the Arduino EEPROM attached with the harvester with ID P2110B004.

On the other hand, the main program in the flash memory takes the structure recorded in the EEPROM and uses these values to execute its functions and print the power obtained from the ADS1115 converter.

#### Arduino Main Program

Figure 4.13 illustrates the structure of the main program in the flash memory of the microcontroller in charge of the reading and communication between ADC and PC. The structure of the code starts with the header, the global variables and function declaration, the main loop, and the functions.

```

1
2 #include <EEPROM.h> // EEPROM libraries
3 #include <string.h>

5 //structure to be uploaded in the EEPROM
6 struct ardEEPROM {
7   char ID[10];
8   float resistor;
9   char date[11];
10  };
11
12 void setup() {
13   Serial.begin(9600);
14   while (!Serial) {
15   }
16   int eeAddress = 0; //location in the EEPROM memory
17   //Data to store.
18   ardEEPROM toArd = {
19     "P2110B004",
20     286.1f,
21     "17.08.2018",
22   };
23   EEPROM.put(eeAddress, toArd);
24 }
25
26 void loop() {
27   /* Empty loop */
28 }

```

**Program 4.2** Program to write in the electronically erasable programmable read-only memory (EEPROM) in the Arduino.

The main loop in the program takes the global variables with the parameters from the EEPROM and read the values from the ADC. Then, it calculates the power and delivers the data to the computer through the serial connection. According to the value read from the ADS1115, the main loop calls the function to change the PGA of the ADC (if necessary). The I<sup>2</sup>C connection between the Arduino and the ADC supports to make changes in the PGA and also to select which input of the ADC to read.

**Table 4.10** Example of the Arduino serialprint.

	Identifier	ADC Port	Power Harvested(mW)
Example	P1110B001	:00	01.123456789012345

The string array printed by the Arduino is read in the program according to the position of the digits, shown in Table 4.10. For example, the ten first digits until the colon symbol (:) is the ID, the two following digits give the ADC input port which reads the voltage in the EVB, and the final digits represent the power calculated

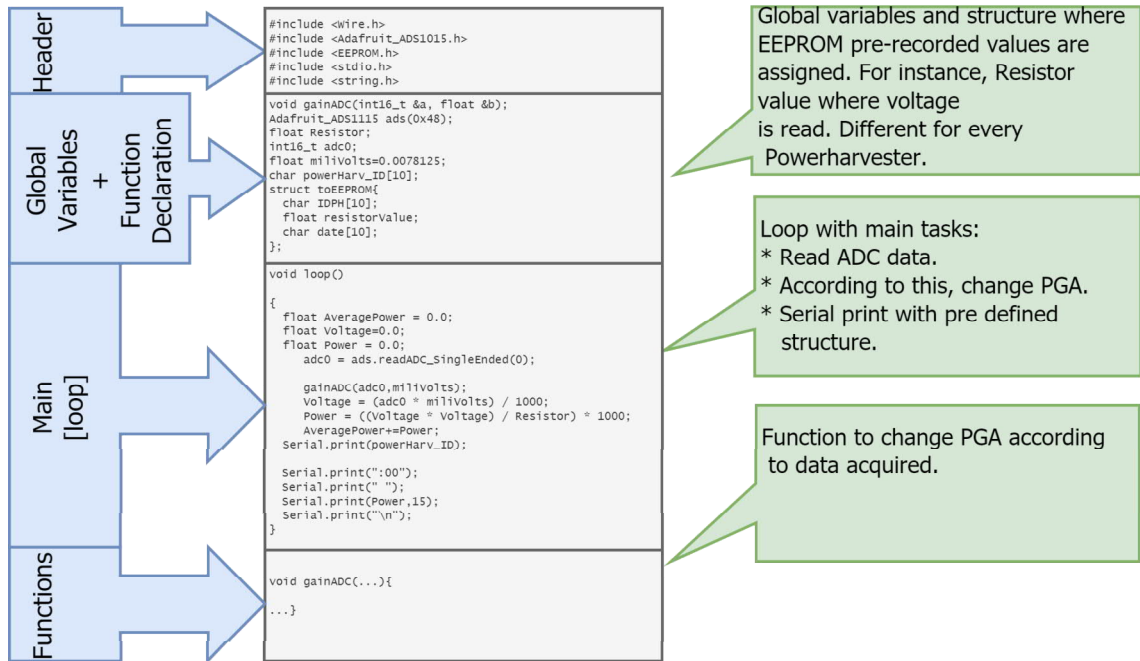


**Figure 4.13** The structure of the Arduino main program has three primarily sections: global variables, main loop, and the functions. The program is loaded in the microcontroller flash memory and takes parameters loaded in the EEPROM.

with the resistor value and the voltage obtained. The ADC port digits can change if more RF-to-DC converters are connected with the same ADC.

## 5. TESTBED FUNCTIONALITY

In order to run operational tests using the implemented testbed a certain sequence of instructions must be followed. This chapter explains how to start an appropriate configuration of parameters, mode selection, the execution of the program, and the acquired data at the output. Section 5.1 explains the structure of the file in which the parameters of the testbed can be configured before the transmission. Section 5.2 explains how the file transmission mode and its operation is selected. Similarly, Section 5.3 describes the operation mode of the vector transmission mode. Finally, the program execution and the outputs acquired after a successful execution are presented in sections 5.4 and 5.5, respectively.

### 5.1 Setting Parameters

To change and set different values related to the transmission there is a configuration file called `Parameters_USRP.txt` in the same folder where the main program code is allocated. This file works as an interface for the user, and also to have a record of the values that the testbed is running. Besides, the settings to choose the operational mode of the testbed can be selected as well. The structure of the file in which the configuration is conducted has three columns: the parameter description, the value, and the default parameter if no value is selected (or if it is not valid).

```
Parameters_USRP.txt    for project_usrp.cpp <<FILE TRANSMISSION MODE BY DEFAULT>>
```

[PARAMETERS]	[VALUE]	[DEFAULT_VALUE]
[0]Sample_type(e.g:short,float,double)	double	double
[1]samples_per_buffer	10000	10000
[2]sample_rate	10e6	500000
[3]center_frequency_in_HZ	915e6	100000000
[4]Gain	80	9
[5]Directory	../Data_Files	../Data_Files
[6]bandwidth	20e6	40e6
[7]Transmit_N_times	1000	1
[8]Transmit_only_file	-	-
[9]Save_samples_in_CSV_file(ON/OFF)	ON	OFF
*****[VECTOR TRANSMISSION MODE]*****		
[11]MODE<VECTOR_TRANSMISSION>(ON/OFF)	OFF	OFF
[12]Repeat_transmission_until_ctr+c(ON/OFF)	ON	OFF
[13]SUBMODE:ITERATION(ON/OFF)	OFF	OFF
[14]Iterative_Window(>100)	100	100

**Figure 5.1** Configuration file where user can change or set different transmission values. Additionally, in the file can be selected the mode of transmission and other related mode functions.

On one hand, there are five parameters connected directly with the USRP transmission values, such as the bandwidth, the gain, the samples per buffer, the sample rate, and the sample type. On the other hand, other values can be set to change parameters related to the file transmission mode or the vector transmission mode.

By default the testbed is set in file transmission mode, unless is changed in the `Parameters_USRP.txt` file. Moreover, the default values are in the third column for unsuitable value selection. For instance, if the value in the second column is "-", the program will use the default value in the third column.

The main program configures the testbed with the values written in the parameter file. Besides, according to the column and the row location, the main program knows how to handle and distribute all the values written and saved in the `Parameters_USRP.txt`. Therefore, in case of changing the format in the configuration file, the entire program may fail and errors may occur.

The main advantage of considering an external file with the parameters is to avoid unnecessary compilation of the program, is easy for the user to change values, and gives default values in case of errors in the selected ones.

## 5.2 File Transmission Mode

The file transmission mode is implemented for broadcasting one or numerous files in a folder. The configuration file must include the folder name and location in order to send the files with waveforms. In Fig. 5.1 the selection of the folder can be seen in row five (`Directory`). Furthermore, the transmission of only one file in the selected folder can be done by adding the name of the file in row eight (`Transmit_only_file`).

The file format are DAT files, files with extension `.dat`, which store bits representing the waveform. For example, the files for operational assessments of the testbed (in Chapter 6), were created in MATLAB and saved as a DAT file. The implemented code for saving a signal is shown Program 5.1, where a complex signal in a vector (`complex_tone`) is saved in another vector (`toSend`) by alternating real and imaginary values, and the vector carrying alternate values (`toSend`) is saved in a file with extension `.dat`.

In addition, there is an option to transmit every file in the folder, or an specific file N times. The number of transmission can be modified in row seven in the `Parameters_USRP.txt` file (`Transmit_N_times`). The number of N transmission

```

1      % Separate real and imag part of x to be written
3      %in binary file
      toSend = zeros(2*length(complex_tone),1);
5      for ii = 1:length(complex_tone)
          toSend(2*ii-1,1) = real(complex_tone(ii));
7          toSend(2*ii,1)   = imag(complex_tone(ii));
      end
9      % Write symbol vector to binary file
      file    = 'complex_tone_double_1M.dat';
11     fileID = fopen(file, 'w');
      fwrite(fileID, toSend, 'double');
13     fclose(fileID);

```

*Program 5.1 Code in MATLAB to write a signal in a file type DAT.*

must be higher than 100 if the size of the waveform file is small (e.g. <100MB), this is due the transmission ends before the threads start to receive data about the harvested voltage from the receiver side.

For example, in Program 4.1 is shown the section in the code where the transmission of a file is programmed. The `buffD` factor in the `transmissionfunction` is the file previously saved into a vector. Besides, `LT` variable starts from zero and each transmission finalized adds one to this factor, thus, when `LT` is equaled to the `N` times (selected in the configuration file) the function ends.

The file transmission mode has also the option to save the track of the obtained values from the RF-to-DC converter. The output files and terminal data acquired after the execution of the testbed is discussed in Section 5.5.

### 5.3 Vector Transmission Mode

The vector transmission mode is intended for testing adaptive algorithms that can be implemented in the testbed. For instance, the power harvested after the first broadcast is considered in the second transmission. Thus, if a vector is transmitted, the vector will change in every transmission depending on the values previously obtained.

In Program 5.2 is shown the transmission function is the same as the one used in file transmission mode. However, the main difference is that the thread employed is focused in the acquirement of the average power without saving any track. Once the vector is sent, the average of each thread created is obtained and can be considered in the next broadcast. The threads are spawned and ended for every broadcast.

```

1 future<void> futureObj[sizeVec];
  thread threads[sizeVec];
3 for (int i = 0; i < sizeVec; i++) {
  start_file = std::chrono::steady_clock::now();
5 futureObj[i]=exitSignal[i].get_future();
  threads[i] = thread(&read_serialVectorMode,
7 ports[i],move(futureObj[i]));
  cout<<"Number of Threads started :"<<
9 sizeVec<<string(50,' ')<<endl;

11 do{
    transmissionfunction(tx_stream,vectorWindow,spbVect);
13 counter++;
    if(repeat and delay > 0.0) {
15 this_thread::sleep_for(
      chrono::milliseconds(int64_t(delay*1000)));
17 }
  } while(repeat and not stop_signal_called);
19
  for(int i=0;i<sizeVec;i++){
21 exitSignal[i].set_value();
    threads[i].join(); }

```

*Program 5.2 Extract of the C++ main program for vector transmission mode.*

## 5.4 Program Execution

The code is compiled by the GCC compiler and then created executables can be executed as a command in the terminal, such as `./<name_of_the_executable>`. In case of the testbed implementation, the terminal must be opened at the folder created in step 2 in Table 4.9. In more detail, the beginning of the execution of the program in the terminal is shown in Fig. 5.3.

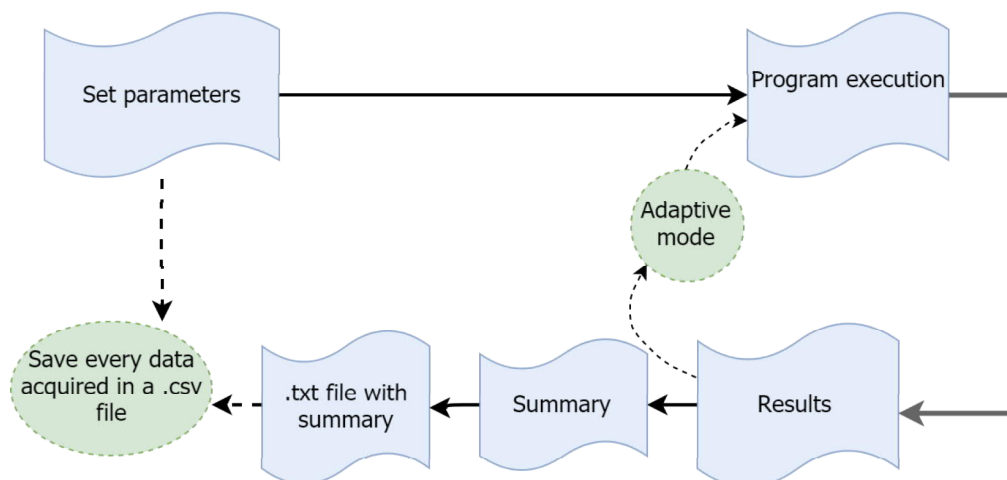


*Figure 5.2 Flow diagram of the testbed program with all the steps shown in terminal display and the resulted outputs.*

The program configures itself with the values stated and saved in `Parameters_USRP.txt`. Furthermore, the setting values at the USRP are shown right after the execution of the program, as well the files in the selected folder and Arduino ports connected, as seen in Fig. 5.3. If it is the first time executing the program when the USRP is connected, the FPGA firmware is loaded as a default image in the SDR.

```

sdr@sdr1:~/MFTF/PROJECT/Compilers$ ./project_usrp
Linux; GNU C++ version 7.3.0; Boost_106501; UHD_003.010.003.000-0-unknown

-- Detected Device: B200
-- Operating over USB 3,
-- Detecting internal GPSDO... No GPSDO found
-- Initialize CODEC control...
-- Initialize Radio control...
-- Performing register loopback test... pass
-- Performing CODEC loopback test... pass
-- Setting master clock rate selection to 'automatic'.
-- Asking for clock rate 16.000000 MHz...
-- Actually got clock rate 16.000000 MHz.
-- Performing timer loopback test... pass

[SETTING PARAMETERS FROM FILE: Parameters_USRP.txt]

Using Device: Single USRP:
Device: B-Series Device
Mboard 0: B200
RX Channel: 0
  RX DSP: 0
  RX Dboard: A
  RX Subdev: FE-RX1
TX Channel: 0
  TX DSP: 0
  TX Dboard: A
  TX Subdev: FE-TX1

Setting TX Rate: 10.000000 Msps...
-- Asking for clock rate 40.000000 MHz...
-- Actually got clock rate 40.000000 MHz.
-- Performing timer loopback test... pass
Actual TX Rate: 10.000000 Msps...

Setting TX Freq: 915.000000 MHz...
Actual TX Freq: 915.000000 MHz...

Setting TX Gain: 80.000000 dB...
Actual TX Gain: 80.000000 dB...

Setting TX Bandwidth: 20.000000 MHz...
Actual TX Bandwidth: 20.000000 MHz...

Checking TX: LO: locked ...

FILES IN DIRECTORY :
-----> complex_tone_double_1M.dat
-----> complex_tone_double_2K.dat
-----> usrp_samples.dat
-----> complex_tone_double_1M_N.dat
-----> sawtooth_double.dat
-----> complex_tone.dat
-----> complex_tone_double.dat
-----> sawtooth_int1.dat

ARDUINO PORTS CONNECTED :
-----> /dev/ttyUSB28
-----> /dev/ttyUSB29
-----> /dev/ttyUSB30
-----> /dev/ttyUSB31

SAVING SAMPLING TRACK IN CSV FILES
-----> ON

TRANSMIT FILE complex_tone_double_2K.dat SELECTED
FILE : ../Data_Files/complex_tone_double_2K.dat

```

**Figure 5.3** Terminal view at the moment when program is setting the values from the configuration file in the USRP.

As seen in Fig. 5.2, there is a loop between the results and the program execution, which occurs in case the vector transmission mode is chosen. The adaptive transmission depends on the values obtained at the results block and adds these values in the program execution block. In the file transmission mode there is no loop and the program flow is only the light blue blocks in Fig. 5.2. The Save every data acquired in a .csv file block (last green oval block at the end of the chain) is optional, and it has to be selected in the first step of the diagram (Set parameters).

A summary text file is created when the execution of the program ends. An optional CSV file to save the data acquired with time tags can be saved if selected in the configuration file, option `save_samples_in_csv_file(ON/OFF)` in Fig. 5.1 (row nine).

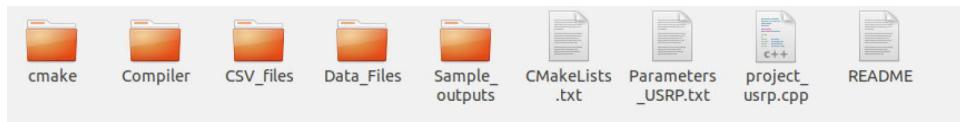


**Figure 5.4** Screenshot of the folder and archives that compound the testbed main program.

## 5.5 Obtained Data

The testbed execution delivers different outputs; the terminal outputs, and the file outputs (summary file and CSV files). There are three folders that are created before the first time the program is executed, the `CSV_files`, the `Sample_outputs`, and the `Compiler`. In the implementation of the testbed the `Compiler` folder is the same as the `build` folder created in step 2 in Table 4.9. In case of the `CSV_files`

```

*****[-----TRANSMISSION IS OVER-----]*****
TOTAL TRANSMISSION TIME : 1.666731 minutes
POWER HARVESTER P1110B001 harvested : 2.23035e-07 mW in average
Total Number of samples ID P1110B001 : 21263

POWER HARVESTER P1110B002 harvested : 2.06389e-07 mW in average
Total Number of samples ID P1110B002 : 21234

POWER HARVESTER P2110B003 harvested : 0.00177116 mW in average
Total Number of samples ID P2110B003 : 21251

POWER HARVESTER P2110B004 harvested : 12.2994 mW in average
Total Number of samples ID P2110B004 : 20921

Total duration for thread with ID P1110B001 : 1.666721 minutes
Total duration for thread with ID P1110B002 : 1.666722 minutes
Total duration for thread with ID P2110B003 : 1.666717 minutes
Total duration for thread with ID P2110B004 : 1.666721 minutes

```

**Figure 5.5** Terminal view after the transmission ends. It is seen how all receivers are listed and with their respected average power generated, duration, and total number of samples.

and the `Sample_outputs` folders, these are created in the first moment when the program starts to set parameters for the USRP, if the folders do not exist already. In addition, the main folder of the program with the files that compose it, can be seen in Fig. 5.4.

The program in the terminal ends with a summary of the transmission, showing the average power measured in all receiver structures connected with the PC. In more detail, in Fig. 5.5, there is a screenshot of the terminal after a transmission in file mode is done. It can be seen also from the figure the total number of samples read in each thread, and are ordered according to the ID in which they are obtained.

```
Summary file for complex_tone_double_2K :

Total duration of file transmission          : 0.965814 seconds
Total number of repetition                  : 10
Used Gain                                   : 80

*****
***** ID P1110B002 *****
Total duration                              : 0.000003 seconds
Average Power harvested                      : -nan [mW]
Diffence between file transmission and data reading : 0.96581053599999997 seconds
Total Number of samples taken                : 0 samples

*****
***** ID P2110B003 *****
Total duration                              : 0.026220 seconds
Average Power harvested                      : 5.64511484e-08 [mW]
Diffence between file transmission and data reading : 0.93959366099999969 seconds
Total Number of samples taken                : 5 samples

*****
***** ID P1110B001 *****
Total duration                              : 0.047169 seconds
Average Power harvested                      : 1.575416324e-07 [mW]
Diffence between file transmission and data reading : 0.91864445299999972 seconds
Total Number of samples taken                : 5 samples

*****
***** ID P2110B004 *****
Total duration                              : 0.094571 seconds
Average Power harvested                      : 2.62492505705714286e-05 [mW]
Diffence between file transmission and data reading : 0.871242406000000025 seconds
Total Number of samples taken                : 21 samples
```

**Figure 5.6** Text file created after the transmission of a file. All acquired values are ordered according to their ID.

The transmission of a file, as for the file mode transmission, gathers all the average power generated in the RF-to-DC converters and prints them in the terminal after transmission. In addition, the program also prints the duration and number of obtained samples .

The summary shown in the terminal once the transmission ends is replicated in a text file. For example, a text file with a summary is presented in Fig. 5.6. The

summary is named after the file transmitted and saved in a dedicated folder for summary outputs (`Sample_outputs`). Additionally, in the summary folder there is another one created within, which includes the date and time of the transmission containing the summary file. Thus, there is a specific folder for each transmission accomplished with the testbed.

Similarly, as the method to save the summary files, CSV files can be created, if the `save_samples_in_csv_file(ON/OFF)` is selected at the configuration text file. Instead of only being named after the transmission file, the CSV files name also contain the identifier from the receiver structure. Besides, the track files are also saved under a new folder created with the date and time when the transmission is conducted. The folder that contains the CSV files is name `CSV_files` and is seen in Fig. 5.4.

## 6. OPERATIONAL ASSESSMENTS

The testbed has primarily two transmission modes and several functions that together generate the outputs. Operational assessments are carried out to prove the correct functionality of all the functions and the results of the implemented testbed.

This chapter summarizes the operational assessments for the testbed in three main sections. Section 6.1 shows the procedure to transmit files containing signals. In a similar manner, Section 6.2 focuses on the vector transmission and how a signal can be created in a vector in order to adaptively modify it. Finally, Section 6.3 describes the results at the receiver side with different gain levels in the transmitter.

The plans to perform tests wirelessly at free bands (868 MHz in Finland) were not possible, because the allowed duty cycle is under 1% [90]. However, the operational assessments in the receiver side were performed through the use of a coaxial cable, as seen in Fig. 6.1. Meanwhile in the operational assessments for the transmission, the USRP was directly connected to a spectrum analyzer.

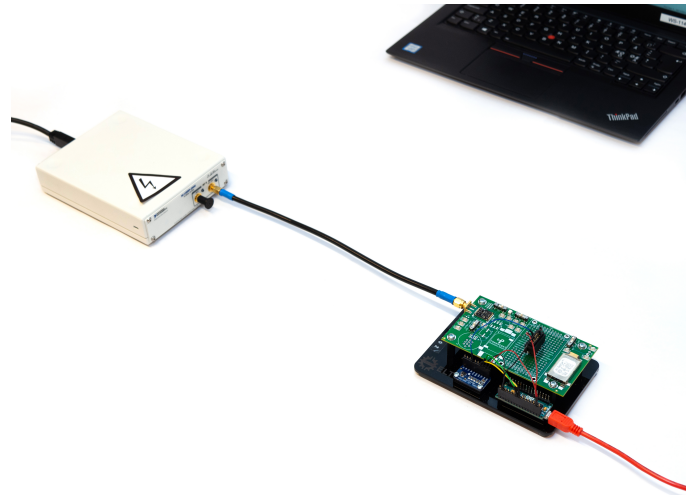


*Figure 6.1* The operational assessments of the testbed were implemented in a wired manner, with a point-to-point connection through a coaxial cable.

## 6.1 File Transmission Assessments

The file transmission assessments were performed in two experiments, the transmission of the same file containing a signal but with different USRP gains, and the transmission of different signal files with the same gain. Besides, measurements are carried out to design a table with the gain level versus the power at the USRP (in dBm), for purposes to have a expected power with certain gain level table meant for calibration.

In the first case, a complex tone signal with 1 MHz is transmitted with different gain levels. Furthermore, the selected center frequency in the USRP is 915 MHz, therefore, the highest peak is expected to be found at 916 MHz. The designed signal at 1 MHz has sample rate of 20 MHz, which must be set in the configuration file (`Sample_rate` in Fig. 5.1). The transmission of the complex tone, shown in the frequency domain in Fig. 6.2, helps for analysis of the obtained waveform in the output of the USRP.

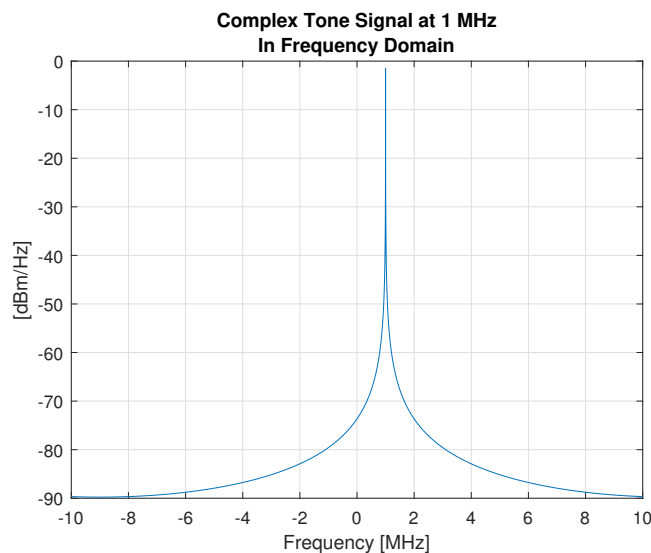
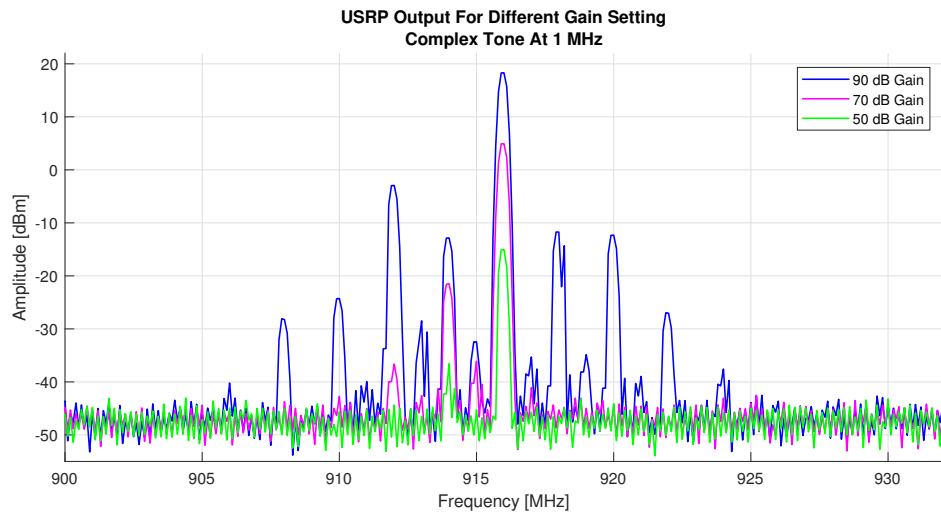
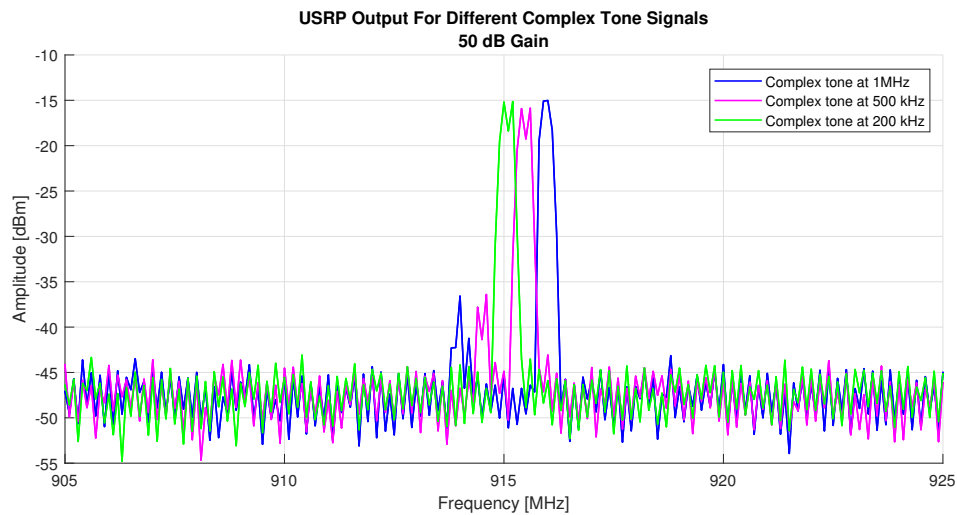


**Figure 6.2** Complex tone used in the tests to prove the correct file transmission mode. In the figure a 1 MHz complex tone is shown in the frequency domain.

The results of the operational assessments carried out to test the transmission of a waveform in the testbed are shown in Fig. 6.3. Figure 6.3(a) illustrates three different tests with the same 1 MHz complex tone signal with different gains (Fig. 6.2). With the highest gain level of 90 dB (blue line), the plot shows higher output power but with many other peaks besides the complex tone at 916 MHz. In the same way, with 70 dB gain (purple line) the output shows a peak in the frequency expected and also with extra peaks, nevertheless, they are considerably fewer than



(a) Same file transmitted with different gain levels



(b) Different files transmitted with same gain level

**Figure 6.3** Output of the USRP for operational assessments for the file transmission mode. A complex tone at 1 MHz is transmitted with different gain levels in (a), and in (b) different complex tone signals with same gain are transmitted.

in the maximum gain case. Finally, at 50 dB (green line), the output does not have any other considerable peak besides the complex tone at the 916 MHz frequency.

As explained in Chapter 3, the values get clipped at the amplification stage in the USRP, which generates harmonic distortion, as seen in the new frequencies next to the complex tone at 916 MHz. Therefore, the nonlinearity region of the system starts approximately at 50 dB, according to the results (Fig. 6.3(a)).

In Fig. 6.3(b), the file transmission mode was tested for sending different files and check the results. As seen in the plot, the same complex tone at 1 MHz (Fig. 6.2)

is sent with 50 dB gain in the USRP, in blue. Additionally, other two files with complex tones are plotted, at 500 kHz in purple and 200 kHz in green. In addition, in Fig. 6.3(b), it is assumed that the neighboring peak to the complex tone is due to I/Q imbalance of the USRP transmitter design.

The output power at certain USRP gain level is shown in Table 6.1, where the measurements were conducted with the transmission of a complex tone file at different gain levels, and measured in the spectrum analyzer.

**Table 6.1** *The output power at the USRP vs the gain selected in the parameters*

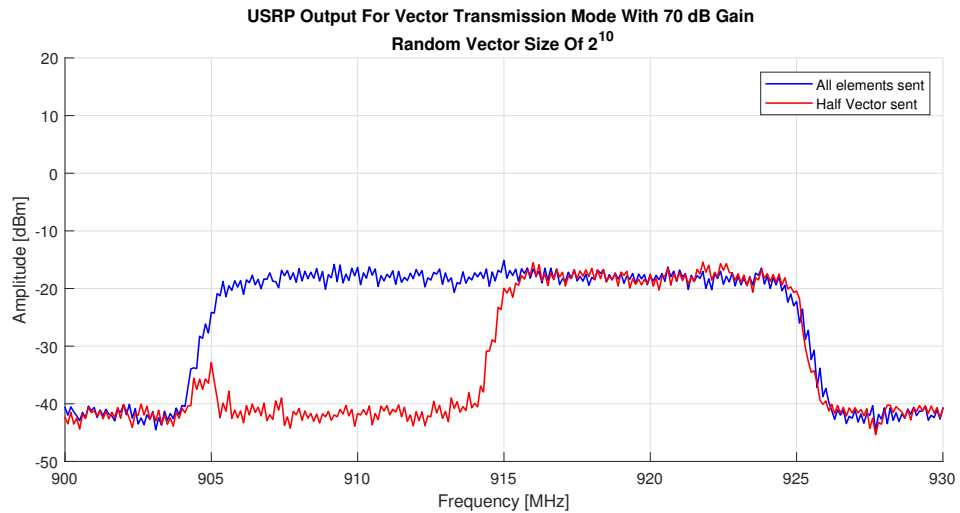
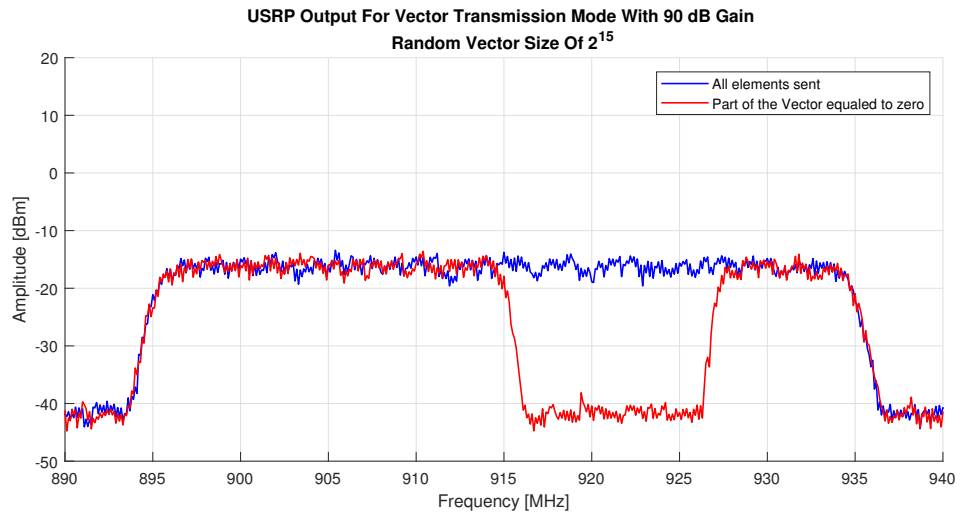
USRP output power (dBm)	Selected gain for transmission (dB)
6	71.50
8	73.75
10	76.00
12	78.00
14	80.00
16	83.25
18	89.75

## 6.2 Vector Transmission Assessments

The vector transmission mode is tested in two ways, the transmission of a vector with each element created randomly in a range of values, and the transmission of a random vector with the same size as previous but with alterations on its elements. Furthermore, the implementation of a transmission employing the whole bandwidth available also is tested, as well changing values at specific ranges in the bandwidth.

The generation of a random vector in the frequency domain is conducted with functions in the testbed main program, as well the IFFT for its time domain representation. The vector carries a complex random signal, thus, the generation of each element in the vector is done between a range (e.g. -1 to 1) with decimal numbers for both the imaginary and the real component. Moreover, the size of the vector must be chosen according to the exponent of two (such as  $2^2$ ,  $2^3$ ,  $2^4$ , and so on) but smaller than 65536 to employ the IFFT function without errors in the execution.

The results are summarized and plotted in Fig. 6.4, where the operational assessments were carried out with two vector sizes and different transmitted bandwidth. In both 6.4(a) and 6.4(b) in order to employed the whole bandwidth, in the parameters file the bandwidth and the sample rate selected are the same. Nevertheless, the results do not have the same gain level configuration.

(a) Transmission of a random vector of size 1024 ( $2^{10}$ )(b) Transmission of a random vector of size 32768 ( $2^{15}$ )

**Figure 6.4** Output of the USRP for operational assessments for the vector transmission mode. It can be observed the transmission in 20MHz and 40MHz bandwidth in (a) and (b) respectively. It is also possible to visualize, in red lines in both plots, the modification of certain elements in the vectors.

In 6.4(a) is seen the comparison between two transmitted vectors with the same gain (70 dB) and size ( $2^{10}$ ). The difference lies in the suppression of specific elements in one of the vector (red line), half of the elements are equaled to zero. The transmission is set in 20 MHz bandwidth and the same value for the sample rate of the vectors transmitted. Therefore, the whole 20 MHz bandwidth is expected to be employed in the transmission of the vector with all the elements and half of the bandwidth employed for the other with half elements equaled to zero, as seen in Fig 6.4(a).

Similarly, Fig. 6.4(b) is conducted, but with 40 MHz for bandwidth and sample

rate, and a higher number of vector elements ( $2^{15}$ ). In this operational assessment only approximately a third of the total elements were equaled to zero, resulting in a gap in between (red line). Whereas, the random vector with all its elements still utilized the whole bandwidth available (blue line).

### 6.3 Receiver Side Assessments

The operational assessments at the receiver side are conducted with a point to point wired connection between the transmitter and one receiver, as in Fig. 6.1. Moreover, the voltage and the current that the USRP takes from the computer were read with the use of the USB cable with parallel connection to a multimeter.

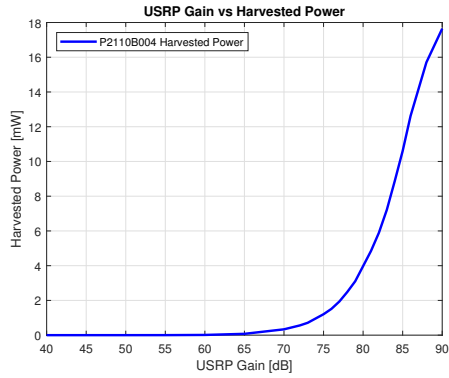
The selected transmission mode was the emission of a file carrying a complex tone at 1 MHz, illustrated in the frequency domain in Fig. 6.2. Other relevant parameters stated at the configuration file are the 1000 times repetition of the waveform and the sample rate at 20 MHz. The employed RF-to-DC converter for operational assessments at the receiver was P2110 EVB, with the identifier P2110B004.

**Table 6.2** Results obtained for operational assessments at the receiver side.

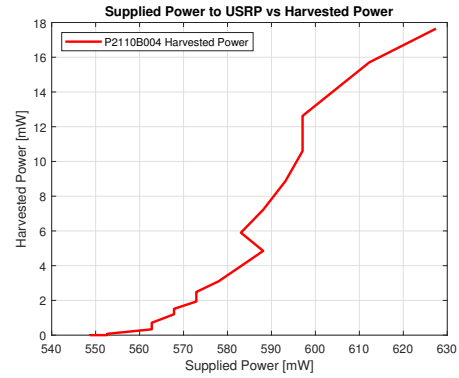
Gain (dB)	Voltage operating (V)	Voltage idle (V)	Current operating (mA)	Current idle (mA)	Power operating (mW)	Power idle (mW)	Harvested power (mW)
Idle	5.15			35		180.25	
40	5.08	5.11	108	79	548.64	403.69	0.00007639
45	5.08	5.10	108	79	548.64	402.90	0.00011350
50	5.08	5.10	108	79	548.64	402.90	0.00031660
55	5.07	5.10	109	80	552.63	408.00	0.00169900
60	5.07	5.10	109	80	552.63	408.00	0.01255000
65	5.07	5.10	109	80	552.63	408.00	0.07616000
70	5.07	5.10	111	81	562.77	413.10	0.33580000
75	5.07	5.10	112	83	567.84	423.30	1.20530000
80	5.07	5.10	115	85	583.05	433.50	3.97400000
85	5.06	5.10	118	87	597.08	443.70	10.6030000
90	5.06	5.09	124	93	627.44	473.37	17.6470000

The results are summarized in Table 6.2, where the first column states the different gain levels in which the tests were executed. The other six following columns tell the voltage, current and the calculated power that the PC supplies to the USRP. The final column is the average power harvested in the receiver side. In the first row the values are for the loading stage of the default FPGA image in the USRP, which happens the first time the program runs. In case of the supplied power from the computer, there are two states of the system, idle and operating stage. The idle stage is when the testbed is not transmitting and waiting for instructions. The operating stage is when the testbed is transmitting, and acquiring data from the receiver.

The results are shown in Fig. 6.5, where the results from Table 6.2 are plotted. The fast increment in the harvested power at the receivers with high USRP gain is seen in Fig. 6.5(a). Similarly, in Fig. 6.5(b) the harvested power curve also increases according to the supplied power from the computer.



(a) USRP gain versus the harvested power at the receiver side



(b) Supplied power from the pc to the USRP versus the harvested power at the receiver side

**Figure 6.5** Representation of the results in the operational assessments for the receiver side. In (a) the fast increment of the harvested power in the receiver side versus the USRP gain is shown. On the other hand, the results of the comparison between supplied power to the USRP and the harvested power are illustrated in (b).

## 7. CONCLUSIONS

Current research shows that wireless power transfer (WPT) is a viable method to deliver energy for electronic devices in upcoming technologies, such as IoT, WSN and 5G. The power transfer through electromagnetic waves has evolved from early experiments since more than 100 years, from everyday gadgets to big scale MPT implementations (i.e. RFID tags, SHARP, and solar power satellites). However, the conducted research in the RF WPT has so far mainly focused on the improvement of separate functional blocks in the WPT chain (e.g. RF-to-DC conversion at the rectenna). There are multiple important elements that must be considered jointly to enhance the end-to-end system efficiency, such as the waveform of the transmitted signal and the wireless channel between a transmitter and a receiver.

A closed-loop system can be used for conducting research on the transmission of waveforms for different purposes, such as communications, power transfer, or SWIPT. Experiments with adaptive algorithms can help in the development of optimized waveforms jointly increasing the efficiency of the block elements in a WPT system. Therefore, the developed testbed in this thesis can be used for future research in the optimization of waveforms, and to implement adaptive algorithms for closed-loop transmissions, and jointly improve the end-to-end efficiency of the system.

The testbed achieves the transmission of any given waveform using a USRP, it harvests the signal into DC voltage and reads these values as digital data through an ADC (ADS1115 16 bits) and microcontroller (Arduino Nano) connection. The central element of the testbed is a computer (Linux OS) with the main program which was developed in C++ for the transmission, and at the same time to read from Arduino Nano the harvested voltage at the RF-to-DC. The testbed has two working modes, the transmission of a waveform in a data file (.DAT), and the transmission of a vector which can be modified in an adaptive algorithm in the main code.

The validation of the testbed was performed under operational assessments, for both working modes in the transmitter and the harvested voltage at the receiver side. In the file transmission mode, the results showed that the system can transmit

any file carrying a waveform which is saved as a data file (.DAT). For example, the transmission of a complex tone at different frequencies and with different gain levels showed to be as expected at the USRP output.

In the vector transmission mode, if a vector is generated (i.e. randomly or with a previously stated signal) the broadcast can be performed and the vector elements can be changed afterwards according to the generated power from the signal. Results showed that it is feasible to transmit a random generated vector, simulating Gaussian noise, and to change it to obtain different transmitted bandwidth in the USRP output.

Furthermore, it is proved that the acquired data in the testbed is the same as the values seen from scientific research equipment (i.e. spectrum analyzer), such as, the harvested power at the receivers, and supplied power from the computer to the SDR. The acquirement and creation of files with summary, and also CSV files to track the receiver performance work as expected. Therefore, the documentation of the results after the execution are straightforward and easy to read for the user.

### **Future Work**

Although the testbed could not be tested wirelessly, the use of an anechoic chamber could be considered with the receiver structures placed in separate locations. Regarding the wireless implementation in an anechoic chamber, a PA must be taken into account to achieve more power in the USRP output. The amplification can be done in the linear region of the USRP, as stated in the operational assessments of the testbed.

As for the the USRP output, it can be considered a power splitter (also called power divider) before the transmitting antenna, to create a parallel connection to scientific research equipment. For example, to have a spectrum analyzer connected with the output signal and the spectrum analyzer connected via USB protocol with the testbed computer. The connection would allow more accurate knowledge of the output power from the USRP and the spectra of the waveform at the moment of transmission only with distortion due to the system (i.e. the PA).

Further research could explore a single input multiple output (SIMO) methodology, which would take advantage of the fact that the testbed main program can handle multiple receiver structures (e.g. not only the four structures implemented for the thesis, but up to 100 if the computer has sufficient memory). It is possible to add more USRPs working as transmitters and generate a multiple input multiple output

(MIMO) system. Also, for purposes to study SWIPT systems and conduct research in the data rate and power optimization, a second USRP can be connected as a receiver. The USRPs can be added with their addresses in the main program and be configured as transmitter and receiver.

The testbed supports any other designed rectenna that can give the DC voltage as the RSSI mode in the P2110 and P1110 EVBs. Therefore, the EVBs used in the testbed can be replaced or simplified with new or different rectenna models, and connected with the ADS1115 ADC converter and Arduino Nano at the receiver structures. As for the testbed software, small changes are necessary to do, particularly, to change parameters in the Arduino Nano EEPROMs. For instance, in the EEPROM of the Arduino Nano in the receiver structure new data is written, such as measured resistor in the new proposed rectenna, the new proposed ID, and the ADC port selected as the input for the analog voltage.

In conclusion, the testbed works as planned with all the designed functionalities. Even though it can be improved upon, particularly with the addition of more hardware, this testbed can support cutting-edge scientific research on improving the end-to-end efficiency of WTP and SWIPT systems through manipulation of the transmitted waveform. Furthermore, the designed C++ program can be used for future projects based on USRP transmission and the simultaneous acquisition of Arduino microcontrollers.

## BIBLIOGRAPHY

- [1] Y. Zeng, B. Clerckx, and R. Zhang, “Communications and signals design for wireless power transmission,” *IEEE Transactions on Communications*, vol. 65, no. 5, pp. 2264–2290, 2017.
- [2] K. Huang, C. Zhong, and G. Zhu, “Some new research trends in wirelessly powered communications,” *IEEE Wireless Communications*, vol. 23, no. 2, pp. 19–27, 2016.
- [3] J. R. Smith, *Wirelessly powered sensor networks and computational RFID*. Springer Science & Business Media, 2013.
- [4] B. Clerckx, R. Zhang, R. Schober, D. W. K. Ng, D. I. Kim, and H. V. Poor, “Fundamentals of wireless information and power transfer: From rf energy harvester models to signal and system designs,” *arXiv preprint arXiv:1803.07123*, 2018.
- [5] R. Weinstein, “Rfid: a technical overview and its application to the enterprise,” *IT professional*, vol. 7, no. 3, pp. 27–33, 2005.
- [6] B. Clerckx, “Wireless information and power transfer: Nonlinearity, waveform design and rate-energy tradeoff,” *IEEE Wireless Communications*, 2016.
- [7] H. J. Visser and R. J. Vullers, “Rf energy harvesting and transport for wireless sensor network applications: Principles and requirements,” *Proceedings of the IEEE*, vol. 101, no. 6, pp. 1410–1423, 2013.
- [8] B. Clerckx and E. Bayguzina, “Waveform design for wireless power transfer,” *IEEE Wireless Communications*, 2016.
- [9] V. Jones. (2010) Heinrich hertz’s wireless experiment (1887). [Online]. Available: [http://people.seas.harvard.edu/~jones/cscie129/nu\\_lectures/lecture6/hertz/Hertz\\_exp.html](http://people.seas.harvard.edu/~jones/cscie129/nu_lectures/lecture6/hertz/Hertz_exp.html)
- [10] A. B. Reeve, “Tesla and his wireless age,” *Popular Electricity*, vol. 4, no. 2, p. 97, Jun 1991.
- [11] W. C. Brown, “The history of power transmission by radio waves,” *IEEE Transactions on microwave theory and techniques*, vol. 32, no. 9, pp. 1230–1242, 1984.
- [12] H.Hertz, *Dictionary of Scientific Biography*. New York:Scribner, 1983, vol. VI.

- [13] A. B. Carlson, P. B. Crilly, and J. Ruttledge, "Communication systems. an introduction to signals and noise in electrical engineering," 1986.
- [14] H. A. Boot and J. T. Randall, "Historical notes on the cavity magnetron," *IEEE Transactions on electron devices*, vol. 23, pp. 724–729, 1976.
- [15] W. C. Brown, "A survey of the elements of power transmission by microwave beam," in *IRE International Convention Record*, vol. 9, no. 3, 1961, pp. 93–105.
- [16] R. George and E. Sabbagh, "An efficient means of converting microwave energy to dc using semiconductor diodes," *Proceedings of the IEEE*, vol. 51, no. 3, pp. 530–530, 1963.
- [17] W. Brown, J. Mims, and N. Heenan, "An experimental microwave-powered helicopter," in *1958 IRE International Convention Record*, vol. 13. IEEE, 1966, pp. 225–235.
- [18] Z. Harouni, L. Cirio, L. Osman, A. Gharsallah, and O. Picon, "A dual circularly polarized 2.45-ghz rectenna for wireless power transmission," *IEEE Antennas and Wireless Propagation Letters*, vol. 10, pp. 306–309, 2011.
- [19] W. Brown, "The combination receiving antenna and rectifier," *Microwave Power Engineering*, vol. 2, pp. 273–275, 1968.
- [20] S. Sasaki, K. Tanaka, and K.-i. Maki, "Microwave power transmission technologies for solar power satellites," *Proceedings of the IEEE*, vol. 101, no. 6, pp. 1438–1447, 2013.
- [21] R. T. Hitchcock, *Radio-frequency and microwave radiation*. AIHA, 2004.
- [22] S. S. Mohammed, K. Ramasamy, T. Shanmuganantham *et al.*, "Wireless power transmission—a next generation power transmission system," *International Journal of Computer Applications*, vol. 1, no. 13, pp. 100–103, 2010.
- [23] R. Mehrotra, "Cut the cord: wireless power transfer, its applications, and its limits," *cse. wustl. edu*, 2014.
- [24] P. Koert and J. Cha, "35 ghz rectenna development," in *Proc. 1st Annu. Wireless Power Transmission Conf., San Antonio, TX*, 1993, pp. 457–466.
- [25] L. W. Epp, A. R. Khan, H. K. Smith, and R. P. Smith, "A compact dual-polarized 8.51-ghz rectenna for high-voltage (50 v) actuator applications," *IEEE Transactions on Microwave Theory and Techniques*, vol. 48, no. 1, pp. 111–120, 2000.

- [26] T.-W. Yoo and K. Chang, "Theoretical and experimental development of 10 and 35 ghz rectennas," *IEEE Transactions on Microwave Theory and Techniques*, vol. 40, no. 6, pp. 1259–1266, 1992.
- [27] C. R. Valenta and G. D. Durgin, "Rectenna performance under power-optimized waveform excitation," in *RFID (RFID), 2013 IEEE International Conference on*. IEEE, 2013, pp. 237–244.
- [28] T. Agarwal. (2016) Schottky diode working and applications. [Online]. Available: <https://www.elprocus.com/schottky-diode-working-and-applications/>
- [29] M. V. Reddy, K. S. Hemanth, and C. V. Mohan, "Microwave power transmission—a next generation power transmission system," *IOSR Journal of Electrical and Electronics Engineering (IOSRJEEE)*, e-ISSN, pp. 2278–1676, 2013.
- [30] M. Onda, N. Kaya, M. Fujita, Y. Fujino, K. Tomita, and M. Yamada, "A stratospheric stationary lta platform concept and ground-to-vehicle microwave power transmission tests," in *37th Aerospace Sciences Meeting and Exhibit*, 1999, p. 1059.
- [31] M. Shwartz, "Wireless power could revolutionize highway transportation, stanford researchers say," Feb 2012. [Online]. Available: <https://news.stanford.edu/news/2012/february/wireless-vehicle-charge-020112.html>
- [32] N. Shinohara, Y. Kubo, and H. Tonomura, "Mid-distance wireless power transmission for electric truck via microwaves," in *Electromagnetic Theory (EMTS), Proceedings of 2013 URSI International Symposium on*. IEEE, 2013, pp. 841–843.
- [33] V. Choudhary, S. P. Singh, V. Kumar, and D. Prashar, "Wireless power transmission: an innovative idea," *International Journal of Educational Planning & Administration*, vol. 1, no. 3, pp. 203–210, 2011.
- [34] B. Clerckx, A. Costanzo, A. Georgiadis, and N. B. Carvalho, "Toward 1g mobile power networks: Rf, signal, and system designs to make smart objects autonomous," *IEEE Microwave Magazine*, vol. 19, no. 6, pp. 69–82, 2018.
- [35] S. Hemour and K. Wu, "Radio-frequency rectifier for electromagnetic energy harvesting: Development path and future outlook," *Proceedings of the IEEE*, vol. 102, no. 11, pp. 1667–1691, 2014.

- [36] S. U. Ay, "A cmos energy harvesting and imaging (ehi) active pixel sensor (aps) imager for retinal prosthesis," *IEEE transactions on biomedical circuits and systems*, vol. 5, no. 6, pp. 535–545, 2011.
- [37] E. Falkenstein, M. Roberg, and Z. Popovic, "Low-power wireless power delivery," *IEEE Transactions on microwave theory and techniques*, vol. 60, no. 7, pp. 2277–2286, 2012.
- [38] Z. Popovic, "Cut the cord: Low-power far-field wireless powering," *IEEE Microwave Magazine*, vol. 14, no. 2, pp. 55–62, 2013.
- [39] "wipe wireless power transmission for sustainable electronics." [Online]. Available: <http://www.cost-ic1301.org/>
- [40] N. B. Carvalho, A. Georgiadis, A. Costanzo, H. Rogier, A. Collado, J. A. García, S. Lucyszyn, P. Mezzanotte, J. Kracek, D. Masotti *et al.*, "Wireless power transmission: R&d activities within europe," *IEEE Transactions on Microwave Theory and Techniques*, vol. 62, no. 4, pp. 1031–1045, 2014.
- [41] F. H. Raab, P. Asbeck, S. Cripps, P. B. Kenington, Z. B. Popovic, N. Pothecary, J. F. Sevic, and N. O. Sokal, "Power amplifiers and transmitters for rf and microwave," *IEEE transactions on Microwave Theory and Techniques*, vol. 50, no. 3, pp. 814–826, 2002.
- [42] D. Masotti, A. Costanzo, M. Del Prete, and V. Rizzoli, "Time-modulation of linear arrays for real-time reconfigurable wireless power transmission," *IEEE Transactions on Microwave Theory and Techniques*, vol. 64, no. 2, pp. 331–342, 2016.
- [43] T. Takahashi, T. Mizuno, M. Sawa, T. Sasaki, T. Takahashi, and N. Shinohara, "Development of phased array for high accurate microwave power transmission," in *Microwave Workshop Series on Innovative Wireless Power Transmission: Technologies, Systems, and Applications (IMWS), 2011 IEEE MTT-S International*. IEEE, 2011, pp. 157–160.
- [44] R. Y. Miyamoto and T. Itoh, "Retrodirective arrays for wireless communications," *IEEE Microwave Magazine*, vol. 3, no. 1, pp. 71–79, 2002.
- [45] A. Costanzo and D. Masotti, "Smart solutions in smart spaces: Getting the most from far-field wireless power transfer," *IEEE Microwave Magazine*, vol. 17, no. 5, pp. 30–45, 2016.

- [46] H. Sakaki and K. Nishikawa, "Broadband rectifier design based on quality factor of input matching circuit," in *Microwave Conference (APMC), 2014 Asia-Pacific*. IEEE, 2014, pp. 1205–1207.
- [47] M. S. Trotter, J. D. Griffin, and G. D. Durgin, "Power-optimized waveforms for improving the range and reliability of rfid systems," in *RFID, 2009 IEEE International Conference on*. IEEE, 2009, pp. 80–87.
- [48] A. S. Boaventura and N. B. Carvalho, "Maximizing dc power in energy harvesting circuits using multisine excitation," in *Microwave Symposium Digest (MTT), 2011 IEEE MTT-S International*. IEEE, 2011, pp. 1–4.
- [49] C. R. Valenta, M. M. Morys, and G. D. Durgin, "Theoretical energy-conversion efficiency for energy-harvesting circuits under power-optimized waveform excitation," *IEEE Transactions on Microwave Theory and Techniques*, vol. 63, no. 5, pp. 1758–1767, 2015.
- [50] A. Collado and A. Georgiadis, "Optimal waveforms for efficient wireless power transmission," *IEEE Microwave and Wireless Components Letters*, vol. 24, no. 5, pp. 354–356, 2014.
- [51] A. Dolgov, R. Zane, and Z. Popovic, "Power management system for online low power rf energy harvesting optimization," *IEEE Transactions on Circuits and Systems I: Regular Papers*, vol. 57, no. 7, pp. 1802–1811, 2010.
- [52] A. Costanzo, A. Romani, D. Masotti, N. Arbizzani, and V. Rizzoli, "Rf/baseband co-design of switching receivers for multiband microwave energy harvesting," *Sensors and Actuators A: Physical*, vol. 179, pp. 158–168, 2012.
- [53] F. Bolos, J. Blanco, A. Collado, and A. Georgiadis, "Rf energy harvesting from multi-tone and digitally modulated signals," *IEEE Transactions on Microwave Theory and Techniques*, vol. 64, no. 6, pp. 1918–1927, 2016.
- [54] J. Kim, B. Clerckx, and P. D. Mitcheson, "Prototyping and experimentation of a closed-loop wireless power transmission with channel acquisition and waveform optimization," in *Wireless Power Transfer Conference (WPTC), 2017 IEEE*. IEEE, 2017, pp. 1–4.
- [55] B. Clerckx, E. Bayguzina, D. Yates, and P. D. Mitcheson, "Waveform optimization for wireless power transfer with nonlinear energy harvester modeling," in *Wireless Communication Systems (ISWCS), 2015 International Symposium on*. IEEE, 2015, pp. 276–280.

- [56] A. Boaventura, A. Collado, N. B. Carvalho, and A. Georgiadis, “Optimum behavior: Wireless power transmission system design through behavioral models and efficient synthesis techniques,” *IEEE Microwave Magazine*, vol. 14, no. 2, pp. 26–35, 2013.
- [57] B. Clerckx and C. Oestges, *MIMO wireless networks: channels, techniques and standards for multi-antenna, multi-user and multi-cell systems*. Academic Press, 2013.
- [58] J. Xu and R. Zhang, “Energy beamforming with one-bit feedback,” in *Acoustics, Speech and Signal Processing (ICASSP), 2014 IEEE International Conference on*. IEEE, 2014, pp. 3513–3517.
- [59] Y. Huang and B. Clerckx, “Waveform design for wireless power transfer with limited feedback,” *IEEE Transactions on Wireless Communications*, vol. 17, no. 1, pp. 415–429, 2018.
- [60] —, “Large-scale multi-antenna multi-sine wireless power transfer.” Institute of Electrical and Electronics Engineers, 2016.
- [61] P. Grover and A. Sahai, “Shannon meets tesla: Wireless information and power transfer,” in *Information Theory Proceedings (ISIT), 2010 IEEE International Symposium on*. IEEE, 2010, pp. 2363–2367.
- [62] T. M. Cover and J. A. Thomas, *Elements of information theory*. John Wiley & Sons, 2012.
- [63] R. Zhang and C. K. Ho, “Mimo broadcasting for simultaneous wireless information and power transfer,” *IEEE Transactions on Wireless Communications*, vol. 12, no. 5, pp. 1989–2001, 2013.
- [64] B. Clerckx and E. Bayguzina, “Low-complexity adaptive multisine waveform design for wireless power transfer,” *IEEE Antennas and Wireless Propagation Letters*, vol. 16, pp. 2207–2210, 2017.
- [65] K. Li, C. Yuen, and S. Jha, “Poster: Fair scheduling for energy harvesting wsn in smart city,” in *Proceedings of the 13th ACM Conference on Embedded Networked Sensor Systems*. ACM, 2015, pp. 419–420.
- [66] S. Nikolettseas, T. P. Raptis, A. Souroulagkas, and D. Tsolovos, “Wireless power transfer protocols in sensor networks: experiments and simulations,” *Journal of Sensor and Actuator Networks*, vol. 6, no. 2, p. 4, 2017.

- [67] P. S. Yedavalli, T. Riihonen, X. Wang, and J. M. Rabaey, "Far-field rf wireless power transfer with blind adaptive beamforming for internet of things devices," *IEEE Access*, vol. 5, pp. 1743–1752, 2017.
- [68] X. Fan, H. Ding, S. Li, M. Sanzari, Y. Zhang, W. Trappe, Z. Han, and R. E. Howard, "Energy-ball: Wireless power transfer for batteryless internet of things through distributed beamforming," *Proceedings of the ACM on Interactive, Mobile, Wearable and Ubiquitous Technologies*, vol. 2, no. 2, p. 65, 2018.
- [69] H. Dai, X. Wang, A. X. Liu, F. Zhang, Y. Zhao, and G. Chen, "Omnidirectional chargability with directional antennas," in *Network Protocols (ICNP), 2016 IEEE 24th International Conference on*. IEEE, 2016, pp. 1–10.
- [70] H. Dai, X. Wang, A. X. Liu, H. Ma, G. Chen, and W. Dou, "Wireless charger placement for directional charging," *IEEE/ACM Transactions on Networking (TON)*, vol. 26, no. 4, pp. 1865–1878, 2018.
- [71] E. Davut, O. Kazanci, A. Caglar, D. Altinel, M. B. Yelten, and G. K. Kurt, "A test-bed based guideline for multi-source energy harvesting," in *Electrical and Electronics Engineering (ELECO), 2017 10th International Conference on*. IEEE, 2017, pp. 1267–1271.
- [72] Y. Wang and G. Cao, "Achieving full-view coverage in camera sensor networks," *ACM Transactions on Sensor Networks (TOSN)*, vol. 10, no. 1, p. 3, 2013.
- [73] E. A. Lee and D. G. Messerschmitt, *Digital communication*. Springer Science & Business Media, 2012.
- [74] "What is i/q data?" Sep 2018. [Online]. Available: <http://www.ni.com/tutorial/4805/en/#top>
- [75] R. v. Nee and R. Prasad, *OFDM for wireless multimedia communications*. Artech House, Inc., 2000.
- [76] J. G. Proakis, M. Salehi, N. Zhou, and X. Li, *Communication systems engineering*. Prentice Hall New Jersey, 1994, vol. 2.
- [77] K. Hill, "What is 64 qam?" Sep 2016. [Online]. Available: <https://www.rerwireless.com/20160901/test-and-measurement/what-is-64-qam-tag6-tag99>
- [78] B. P. Lathi, *Modern digital and analog communication systems*. Oxford University Press, Inc., 1995.
- [79] W. H. W. Tuttlebee, "Software-defined radio: facets of a developing technology," *IEEE Personal Communications*, vol. 6, no. 2, pp. 38–44, April 1999.

- [80] *374924C-01 Software Defined Radio Device Datasheet*, National Instruments, July 2017, available: <http://www.ni.com/pdf/manuals/374924c.pdf>.
- [81] “Yzxstudio usb meter zy1273.” [Online]. Available: <https://lygte-info.dk/review/usbMeterYZXStudioZY1273UK.html>
- [82] *TTL to USB Serial Converter Generic*, Future Technology Devices International Ltd, FTDI Chip, May 2018, available: [https://www.ftdichip.com/Support/Documents/DataSheets/Cables/DS\\_TTL-232RG\\_CABLES.pdf](https://www.ftdichip.com/Support/Documents/DataSheets/Cables/DS_TTL-232RG_CABLES.pdf).
- [83] K. Li, C. Yuen, B. Kusy, R. Jurdak, A. Ignjatovic, S. S. Kanhere, and S. Jha, “Fair scheduling for data collection in mobile sensor networks with energy harvesting,” *arXiv preprint arXiv:1603.02476*, 2016.
- [84] *P2110 – 915 MHz RF Powerharvester<sup>TM</sup> Receiver Datasheet*, Powercast Corporation, August 2015, available: <https://www.powercastco.com/wp-content/uploads/2016/11/p2110-datasheet-rev-b.pdf>.
- [85] *P1110 – 915 MHz RF Powerharvester<sup>TM</sup> Receiver Datasheet*, Powercast Corporation, December 2016, available: <http://www.powercastco.com/wp-content/uploads/2016/12/P1110B-Datasheet-Rev-4.pdf>.
- [86] *Ultra-Small, Low-Power, 16-Bit Analog-to-Digital Converter with Internal Reference*, Texas Instruments, October 2009, available: <https://cdn-shop.adafruit.com/datasheets/ads1115.pdf>.
- [87] ARDUINO. (2018) ARDUINO NANO. [Online]. Available: <https://store.arduino.cc/usa/arduino-nano>
- [88] “Uhd (usrp hardware driver<sup>TM</sup>).” [Online]. Available: <https://www.ettus.com/sdr-software/detail/usrp-hardware-driver>
- [89] “Usrp hardware driver and usrp manual.” [Online]. Available: [https://files.ettus.com/manual/page\\_build\\_guide.html](https://files.ettus.com/manual/page_build_guide.html)
- [90] T. F. C. R. A. (FICORA). (2018) Regulation on collective frequencies for licence-exempt radio transmitters and on their use. [Online]. Available: [https://www.finlex.fi/data/normit/32670/Regulation\\_15AM.pdf](https://www.finlex.fi/data/normit/32670/Regulation_15AM.pdf)